Cl

A MÖSSBAUER AND ADSORPTION STUDY OF Fe^{57} IN LINDE L ZEOLITE

by

RAYMOND TROY LASSAU

B.Sc., University of British Columbia, 1966

A THESIS SUBMITTED IN PARTIAL FULFILMENT OF

THE REQUIREMENTS FOR THE DEGREE OF

MASTERS OF SCIENCE

in the Department

of

Chemistry

We accept this thesis as conforming to

the required standard

THE UNIVERSITY OF BRITISH COLUMBIA

August 31, 1972

In presenting this thesis in partial fulfilment of the requirements for an advanced degree at the University of British Columbia, I agree that the Library shall make it freely available for reference and study. I further agree that permission for extensive copying of this thesis for scholarly purposes may be granted by the Head of my Department or by his representatives. It is understood that copying or publication of this thesis for financial gain shall not be allowed without my written permission.

Department of Chemistry

The University of British Columbia
Vancouver 8, Canada

Date 20/9/72

ABSTRACT

A single Fe^{3+} species has been introduced into Linde L zeolite and is identified as an iron oxyhydroxide from its Mössbauer relaxation properties. The effects of N_2, CO_2 and C_2H_6 on the ferric species and on the bulk behaviour of the sample are observed by Mössbauer Spectroscopy and adsorption studies under outgassing conditions. The ferric oxyhydroxide initially blocks the pores to gas adsorption but reducing it to Fe^{o} at 943°K and reoxidizing it to α-Fe_2O_3 in air at 773°K frees the pores. The bulk α-Fe_2O_3 is concluded to lie on the external zeolite surface.

Acknowledgements:

I would like to thank Dr. J.R. Sams for his patience and guidance during the course of this investigation. I would also like to thank Mrs. L. Sallos, Dr. J. Ruddick and Mr. J.C. Scott for invaluable assistance.

TABLE OF CONTENTS

List of Figures

List of Tables

INTRODUCTION

In the study of solid surfaces many physical tools have been employed. Such techniques as are used in electron microscopy, optical and magnetic resonance spectroscopy, Mössbauer Spectroscopy and sorption studies have contributed substantially to present day knowledge about surface structure and catalytic activity. Of the many varieties of surfaces studied by these methods a large measure of attention has been paid recently to the physical and chemical behaviour of porous materials such as zeolites.

Synthetic zeolites[1,2] consist of tetrahedrally arranged silicates and aluminates bonded by common oxygen atoms. The polyhedra so formed contain large interstitial cavities resulting in highly porous solids with large internal surface areas. The silicon to aluminum ratio varies in different zeolites and hence the number of cations required to balance the residual charge on aluminum also varies. The cations occupy different sites owing to the random replacement of silicon by aluminum. Water molecules occupy the cavities and form hydration complexes with the cations as well as electrostatically interacting with the framework oxygen atoms.

The molecular sieving properties of zeolites have been well established in the literature. Of more recent interest are studies of the centres of catalytic activity on the surface and the changes that occur by including different ions in the zeolitic channels.

When an iron ion is adsorbed from a liquid onto a zeolitic support or ion-exchanged into it, the valence state and type of bonding of the ion to the surface, the symmetry of the electric field surrounding the ion, and the presence and magnitude of a magnetic field are but a few of the many pieces of information that can be obtained by Mössbauer Spectroscopy[3]. If sample evacuation, thermal treatment or the presence of either physically or chemically adsorbed gases affect any of these properties, the Mössbauer Spectra will reflect the changes.

The isomer shift, δ, arises from the interaction between electronic charges and nuclear charges. The magnitude of the shift depends on the size of the nucleus in its ground and excited states and on the s-electron densities ($|\psi(o)|^2$) at the nucleus for the source and absorber. It is given by

$$\delta = \frac{2\pi}{5} Ze^2 \left[|\psi a(o)|^2 - |\psi s(o)|^2\right]\left[R^2_{ex} - R^2_{gd}\right]$$

where Z is the nuclear charge, e the electron charge, R_{ex} and R_{gd} the excited and ground state radii; "a" and "s" denote source and absorber. P and d-electron density influence the isomer shift only through shielding effects of the s-electron density at the nucleus.

In ionic compounds of high spin Fe^{3+} and Fe^{2+}, the presence of an additional d-electron in Fe^{2+} shields the s-electrons from the nucleus to a greater extent than in Fe^{3+}, hence Fe^{2+} has a lower value of $|\psi(o)|^2$. This, coupled with the fact that $(R^2_{ex} - R^2_{gd})$ is negative[4] for Fe^{57} leads to the fact that Fe^{2+} should have a more positive isomer shift than

Fe^{3+}. Thus the valence state of the ion can be identified.

Quadrupole splitting is the result of the interaction between the nuclear quadrupole moment and an electric field gradient (EFG) at the nucleus established by charges in its immediate vicinity. The electric field gradient can arise from non-spherical distribution of the atom's own valence electrons or from neighbouring ion or atom asymmetries. Nuclei with spins $I \geqslant 1$ have quadrupole moments, for example, the first excited state of Fe^{57} where $I = {}^3/2$.

For Fe^{57} the quadrupole splitting is the difference in energy levels between the magnetic quantum states $m_I = \pm{}^3/2$ and $\pm{}^1/2$. The degeneracy of the $I = {}^3/2$ state is partially lifted by the EFG. The quadrupole splitting is given by

$$\Delta E_Q = E_Q({}^3/2) - E_Q(\tfrac{1}{2}) = \tfrac{1}{2} V_{ZZ} eQ \left[1 + \frac{\eta^2}{3}\right]^{1}/2$$

where V_{ZZ} is the Z-component of the EFG tensor, eQ the nuclear quadrupole moment of the first excited state, and η an asymmetry parameter defined by $\eta = (V_{XX} - V_{YY})/V_{ZZ}$. The transition probabilities $\pm\frac{1}{2} \rightarrow \pm\frac{3}{2}$ and $\pm\frac{1}{2} \rightarrow \pm\frac{1}{2}$ are equal for a powdered sample with random orientation of the crystallites and two lines of equal intensity are obtained. Where crystallite orientations are not totally random the angular dependence of the transitions may not average to zero and two lines of unequal intensity will result.

For high spin Fe^{3+} compounds the half-filled d-shell ($3d^5$) is spherically symmetric and hence where a small quadrupole splitting is observed it must arise from the EFG

set up by the arrangement and electronegativities of its nearest neighbour ligands which are either not all chemically identical or which do not have cubic symmetry. For high spin Fe^{2+} the extra d-electron ($3d^6$) contributes much more to the large quadrupole splitting (the EFG is proportional to $\langle r^{-3} \rangle$) than do the ligands[5].

Figure 1a) represents isomer shift and quadrupole splitting and Figure 1b) Zeeman splitting.

Zeeman splitting is the result of an interaction between the nuclear magnetic dipole moment (μ) and a net magnetic field (H) at the nucleus. The energy levels for the interaction are

$$E_m = \frac{-\mu H m_I}{I} = -g\mu_n H m_I$$

where g is the gyromagnetic ratio and μ_n the nuclear magneton. In the absence of any quadrupole interaction there are 2I+1 equispaced levels, the splitting between adjacent levels being $g\mu_n H$. Only six spectral lines result because of the selection rule $\Delta m_I = 0, \pm 1$.

With quadrupole interaction the energies of the different m_I states are shifted. The magnitude of the quadrupole splitting is determined as the difference between the two pairs of outer lines, that is $|\Delta_{12} - \Delta_{56}|$ as is the case with the six-line spectra of α-Fe_2O_3. The sign of the electric field gradient depends on whether $(\Delta_{12} - \Delta_{56})$ is positive or negative.

The asymmetry of quadrupole split lines for a given oxidation state of the absorbing atom has been attributed to

FIGURE 1

Energy level diagram showing:

a. Isomer Shift and Quadrupole Splitting.

b. Nuclear Zeeman Splitting and the effect thereon of Quadrupole Coupling.

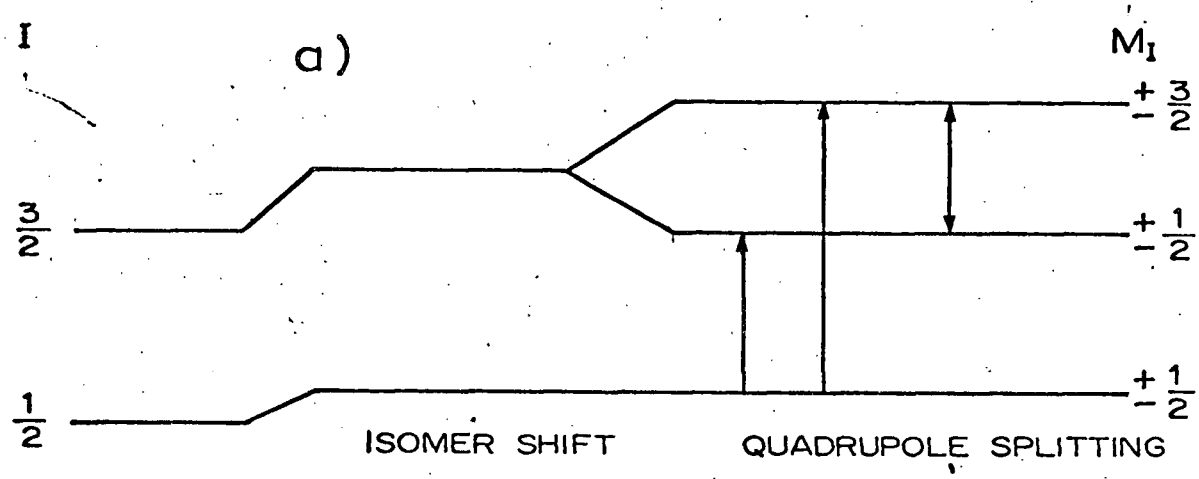
I
a)
M_I
$+\frac{3}{2}$
$-\frac{3}{2}$
$\frac{3}{2}$
$+\frac{1}{2}$
$-\frac{1}{2}$
$+\frac{1}{2}$
$-\frac{1}{2}$
$\frac{1}{2}$
ISOMER SHIFT
QUADRUPOLE SPLITTING

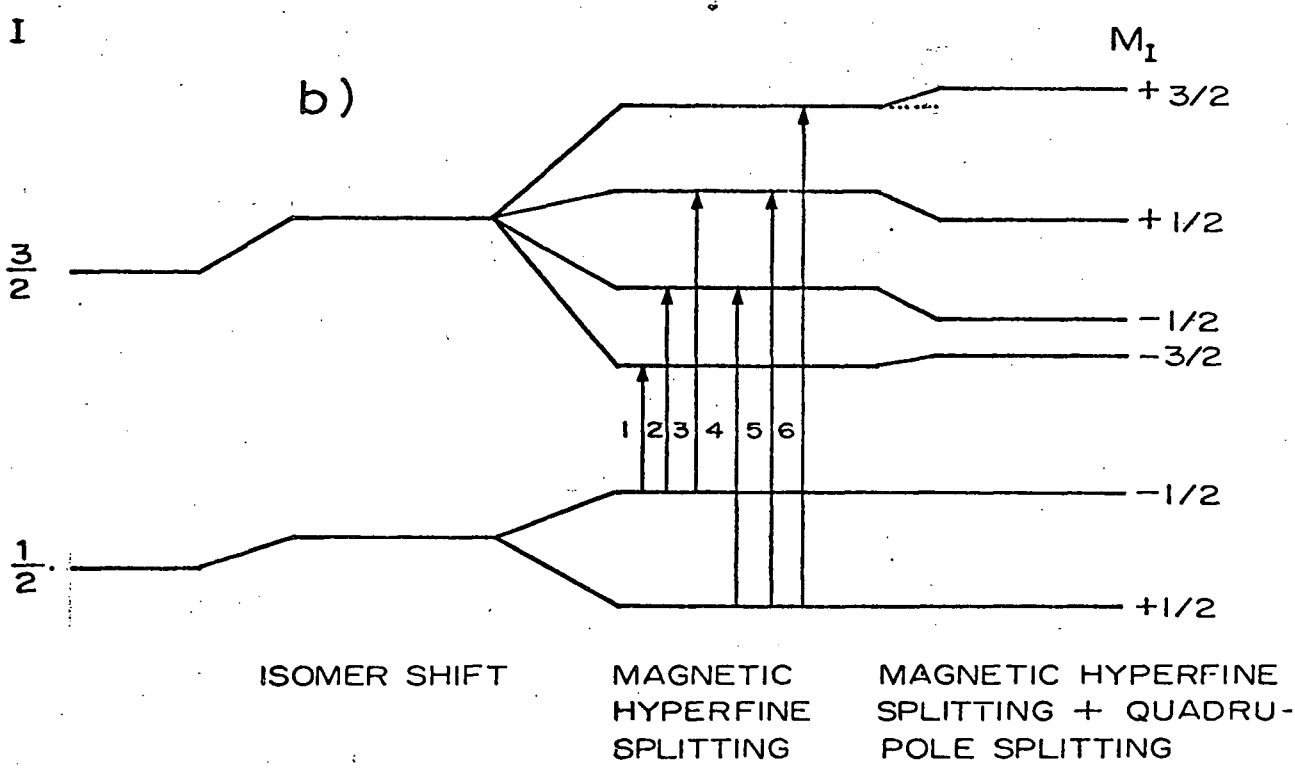
I
b)
M_I
+3/2
+1/2
-1/2
-3/2
3/2
1 2 3 4 5 6
-1/2
1/2
+1/2
ISOMER SHIFT
MAGNETIC HYPERFINE SPLITTING
MAGNETIC HYPERFINE SPLITTING + QUADRUPOLE SPLITTING

two causes: 1) the non-zero averaging of the angular dependence of crystallite orientations (the angle is a function of the direction of orientation of the EFG and γ-ray) as has already been mentioned and 2) the presence of sufficient numbers of crystallites contributing to the Mössbauer effect with anisotropic lattice vibrations[6]. A third and currently very important cause of asymmetry observed in Mössbauer Spectra is attributed to fluctuating electric and magnetic fields generated either as a result of the relaxation of paramagnetic ions or by the fluctuation of the environment surrounding the nucleus[7,8].

Paramagnetic relaxation phenomenon are the result of time-dependent changes in unpaired electron spin directions. The two mechanisms which cause spin-flipping are electronic spin-spin interactions with neighbouring ions and electronic spin-lattice interactions. Both involve the transfer of energy between interacting spins, the former through dipole and exchange spin interactions and the latter through spin-orbit coupling.

Spin-spin relaxation is temperature independent and the relaxation time increases as the distance between paramagnetic centres increases. Spin-lattice relaxation is temperature dependent and the relaxation time increases with decreasing temperature.

If the relaxation time is less than the time taken for a Mössbauer event then the effective magnetic field generated at the nucleus will be zero. Where the relaxation time is

equal to or greater than that for a Mössbauer event a non-zero effective magnetic field will result. Mössbauer spectra show these effects in the following manner. For an Fe^{57} nucleus in a fluctuating magnetic field and a fixed electric field gradient: a) where the rate of fluctuation is slower than the nuclear precession frequency a six-line hyperfine pattern results, b) for extremely rapid fluctuation the six-line pattern collapses inward (motional narrowing) and a symmetrical quadrupole doublet is seen, and c) for intermediate fluctuation rates the $\pm\frac{3}{2} \rightarrow \pm\frac{1}{2}$ transition line which makes up one half of the quadrupole doublet is broader than the other line of the doublet $\left[\begin{matrix}\pm\frac{1}{2} \rightarrow \pm\frac{1}{2} \\ \pm\frac{1}{2} \rightarrow \mp\frac{1}{2}\end{matrix}\right]$ because the relaxation time for the latter component is shorter. Hence an asymmetric quadrupole doublet is seen (line-widths Γ_o are inversely proportional to the half-lives $t_{1/2}$ of the excited states).

The same pattern is generated by relaxation effects in cooperative phenomenon such as ferromagnetism and antiferromagnetism. Techniques other than Mössbauer Spectroscopy (magnetic studies for example) are sometimes necessary to distinguish between ordered magnetic and disordered paramagnetic hyperfine spectra.

The application of Mössbauer Spectroscopy to the study of surfaces yields a great deal of information. In particular, from the adsorption interaction between gas and metal atoms, changes in the isomer shift and the quadrupole splitting reflect changes in the electronic structure of the Mössbauer

atom and produce information about the adsorption complex. However, where ions are introduced into zeolites the degree to which the ions occupy external or internal surfaces is not necessarily discernable from Mössbauer parameters if the sites have similar energies and geometries. Also pore size restrictions on adsorbed gases, surface area and energetics of the bulk material are not obtainable. Adsorption isotherms can provide this information and valuable comparisons can be made between the collected data of both techniques.

When the equilibrium concentration of gas molecules at a solid surface is greater than that in the bulk gas phase the gas adsorbate is interacting with the solid adsorbent.

Adsorption processes are conveniently classified as either physical or chemical depending upon the nature of interaction between adsorbate and adsorbent, and can usually be differentiated by the following criteria: 1) The interaction energies for physical adsorption are of the order of magnitude of those for condensation processes, whereas for chemisorption energies similar to those for bond formation are observed and usually an activation energy barrier must first be overcome. The energies of both types of adsorption can vary appreciably with surface coverage if the adsorbent surface is not homogeneous and under pressure conditions where lateral gas-gas interactions occur. Highly porous solids offer a wide variety of adsorption sites whose energetics can be quite different.

2) Chemisorbed gases are one molecular diameter in thickness over any pressure range whereas multilayer formation is

frequently observed when gases are physically adsorbed at pressures approaching the adsorbate vapor pressure.

3) Physical adsorption is preferred at the adsorbate boiling point. Owing to the kinetic energy of the gas molecules at higher temperatures the volume adsorbed decreases. The activation energy involved in chemisorption results in the reverse of this trend, the higher temperatures being favoured. The rates of adsorption in both cases may be similar if equilibrium depends on diffusion effects inherent in porous adsorbents; otherwise chemical adsorption is slower.

4) Physically adsorbed gases are readily desorbed when the pressure is reduced at the temperature at which adsorption took place, but often high temperatures of outgassing are required to remove a chemisorbed layer.

As the determination of zeolite surface areas is one of the main objectives of this work only physical adsorption will be discussed further.

The number of moles of gas adsorbed on a solid depends on the interaction energy generated between the two phases, on the temperature and pressure and on the area of the solid surface exposed to the gas phase. Plots of the amount of adsorbed gas against equilibrium pressure at a constant temperature (adsorption isotherms) yield qualitative and semi-quantitative information about the adsorption system. From such isotherms estimates of surface area and adsorption energy can be made although the interpretation of these

quantities is subject to the assumptions contained in the model chosen to represent the adsorption process.

For porous materials such as zeolites, if isotherms are determined below the critical temperature of the adsorbate and over a pressure range from a few torr to an atmosphere, multilayer adsorption is usually observed. The multimolecular adsorption theory of Brunauer, Emmett and Teller[9] (BET theory) provides a useful two constant equation from which approximate surface areas and heats of adsorption can readily be evaluated.

The BET theory is based on the following assumptions: 1) The surface possesses uniform, localized sites 2) The adsorption is non-cooperative in that lateral interactions between gas molecules are ignored 3) The energy of adsorption in the first layer E_1, is a constant 4) The energy of adsorption in succeeding layers is E_L, the energy of adsorbate liquefaction and 5) The surface area available for the nth layer is equal to the coverage of the (n-1)th layer. As has been pointed out by detailed criticims[10] of these assumptions, the area and energy parameters have no absolute significance. However, where surface areas are compared on a relative basis using the same adsorbate the theory is quite useful.

The BET isotherm takes the following form

$$v = \frac{v_m C \; P}{(Po-P)\left\{1+(C-1)\left(P/Po\right)\right\}}$$

where v is the volume adsorbed at pressure p, v_m the adsorbate volume required to complete the first adsorbed layer, Po the adsorbate vapor pressure at the experimental temperature T and $C = e^{(E_1-E_L)/RT}$. In order to obtain values for v_m and C

the above equation is rearranged into the following form

$$\frac{Po}{v(Po-P)} = \frac{1}{v_m} + \frac{Po-P}{v_m CP}$$

Thus, plots of $Po/_{v(Po-P)}$ against $(Po-P)/_{p}$ should be linear with $\frac{1}{v_m}$ as the intercept and $\frac{1}{v_m C}$ as the slope.

The value of the surface area A, of the adsorbent is obtained by assuming closest packing of the adsorbate. In fact this is in opposition to the site-wise localized adsorption postulated by the BET theory. This would require that the adsorbent be close-packed and defect free and as well that the adsorbate and adsorbent be precisely matched in size. For hexagonal closest packing of spheres

$$A = 9.322 \times 10^{15} \quad v_m \left(\frac{M}{4\sqrt{2} N\rho} \right)^{2/3} \quad m^2 g^{-1}$$

where M is the adsorbate molecular weight, N Avogadro's number and ρ the density of the liquified gas.

As the interpretation of the value of E_1, obtained from the BET equation is hampered by all the assumptions inherent in the model, arguments about energetics are better based on a thermodynamic quantity. Where isotherms for the same adsorbate-adsorbent system are available at different temperatures, differential heats of adsorption (isoteric heats q_{ST}) can be obtained from an analogue of the Clausius-Clapeyron equation.

$$q_{ST} = -R \left(\frac{\partial \ln p}{\partial {}^{1}/_{T}} \right)_{Na,A}$$

allows the direct determination of adsorption heats from experimental isosteres by plotting lnp against $^{1}/_{T}$ at constant number of moles adsorbed Na. The necessary thermodynamic

relations have been previously derived[11-13] from solution thermodynamics.

Since the charge-compensation cations of zeolites lie in crystallographically well-defined positions an iron-exchanged molecular sieve should have a high fraction of crystallographically well-defined surface Mössbauer atoms. Thus many experimenters have been preparing iron zeolites and examining the iron products so formed. Depending upon the method of preparation, the zeolites are either exchanged or act as supports for the growth of small particles[14,15].

Ferric ions exchanged into zeolites have led to different Mössbauer results. Morice and Rees[16] showed that exchange in X and Y zeolites produced high spin ferric and ferrous species, whereas exchange in L-zeolite by Wedd[17] and co-workers produced a ferric species only. On outgassing this sample the ferrous species was obtained.

Ferric ion-exchange in Y and M zeolites was studied by Goldanskii[18] and co-workers who obtained a Mössbauer doublet characteristic of a ferric species. Adsorption studies were interpreted as producing a ferrous species. The doublet due to this species decreased in intensity with increasing temperature but the ferric doublet appeared impervious to either adsorption processes or temperature changes. They concluded that the ferric ion was strongly bound to the zeolite lattice but the ferrous ion was not.

The asymmetry of the ferric doublet was interpreted as a spin-lattice relaxation effect. Dehydration of the initial

sample also produced a ferrous species.

The following points seem to be characteristic of these samples:

1) Ferric exchange produces a Mössbauer doublet characteristic of a ferric species, although in some cases a ferrous doublet is also observed.
2) Dehydration produces a ferrous species.
3) Adsorption processes appear to affect the ferrous species but not the ferric species.

The above results appear to agree fairly well with the idea that the ferric ions are localized on the lattice and that the ferrous ions are not and in fact appear to be quite mobile.

The purpose of this work was to examine a similar system ($FeCl_3$ in L-zeolite[17]) by Mössbauer Spectroscopy and to look at the adsorption isotherms for the same system. If mobile ions exist in the pores then comparison of the surface area with that of the host zeolite should show a marked change.

The reactivity of the surface toward different gases could be compared with the Mössbauer parameters. In this way the influence of the oxidation state of iron on adsorbed gases could possibly be determined.

If in fact there is more than one species of iron initially in the sample then attempting to convert the species by a reduction process into a single iron species and measuring adsorption isotherms would yield valuable information about the state of aggregation within the pores. The combination

of Mössbauer Spectroscopy and adsorption techniques could then determine the oxidation state of the mobile species during the conversion process and whether the final product remained within the pores or on the external surface.

EXPERIMENTAL

(i) Materials:

Wedd[17] and co-workers found that iron-exchange occurred readily in L-zeolite when the PH of the exchange solution was greater than 2. The sample used for this work was prepared by dissolving stock $FeCl_3 \cdot 6H_2O$ in anhydrous ethyl ether in proportions of 33% weight to volume, centrifuging and decanting the solution then introducing approximately 10 grams of synthetic Linde Molecular Sieve L obtained from Union Carbide of Canada. The slurry was stirred for an hour before it was filtered and washed with ether to a negative KCNS test. The product was again treated in the same manner with a fresh solution of $FeCl_3 \cdot 6H_2O$ in ether. The final product had undergone three such treatments before it was dried in air at 110°C and used for subsequent experiments.

Potentiometric iron analysis was performed on the samples after each solvent addition. The samples were dissolved in concentrated hydrochloric acid and stannous chloride was added to reduce the ferric ion to ferrous ion. The titration was carried out with a ceric sulphate solution previously standardized against ferric ammonium sulphate. Cell emf's were measured on a Beckman PH meter using platinum and saturated calomel electrodes.

The analysis indicated that the quantity of iron increased from 7.5 to 9.5% by weight after each solvent addition and that further treatment did not appear to increase the 9.5% value. However, the identical preparation of two such samples after three solvent additions did not produce identical iron

contents. The first sample contained 9.5% iron and the second 8.1% iron. Possibly the large quantity of ether required to wash the sample to a negative KCNS test was responsible for this variation.

Mössbauer and adsorption studies were conducted on two prepared samples of iron-in-L-zeolite. The second preparation, on which the major portion of this thesis is based, was analysed by Dr. A. Bernhardt at 5251 Elbach über Engelskirchen, West Germany. Table 1 lists the results of the analyses performed by Dr. Bernhardt on L-zeolite, solvated L-zeolite (L-zeolite mixed only with anhydrous ethyl ether but prepared in the above manner) and the second preparation of iron-in-L-zeolite (after three solvent additions).

Adsorption experiments were conducted with L-grade nitrogen supplied by Canadian Liquid Air Co. and research grade carbon dioxide and ethane supplied by Matheson Co. Research grade helium supplied by Matheson was used to determine the adsorption system volumes.

(ii) X-Ray Powder Photographs:

Powder photographs were taken with a Philips powder camera of 11.46 cm diameter. Samples were mounted in 0.5 mm (inside diameter) glass capillaries approximately 5 mm in length. Cu $K\alpha$, λ = 1.54050 Å, X-irradiation was used with a Ni filter to reduce K_β radiation. The film used was Kodak Medical X-Ray (Estar safety base) cut into strips 3.5 X 35.5 cm for use in the camera. To obtain photographs for line position measurements a pinhole collimator was used giving photographs with sharp,

Table 1

SAMPLE	%				
	Si	Al	Fe	Cl	C
1. L-zeolite (no treatment)	23.55	6.89			0.21
2. L-zeolite (after three additions of anhydrous ethyl ether)	24.53	7.29			0.86
3. L-zeolite (after three additions of $FeCl_3 \cdot 6H_2O$ in anhydrous ethyl ether) preparation #2	18.80	5.68	7.99	4.47	0.57

low angle lines. The lines on the photographs were indexed on a light box provided with a meter stick to which was attached a measuring slide assembly containing a vernier and a magnified cross-hair for location of the diffraction line. The d spacings for these lines were then calculated.

(iii) Magnetic Measurements:

Magnetic susceptibility measurements on the samples of iron-in-L-zeolite were made by the Gouy method. The variable temperature susceptibility determinations were made using an electromagnet and semi-microbalance over the temperature range 80^{o} to 300^{o}K and at three field strengths between 4500 and 8000 gauss.

A pyrex gouy tube between 3 and 4 mm inside diameter was used and calibrated with gravimetrically analysed $HgCo(CNS)_4$. The susceptibility values reported are the average of two Gouy tube sample packing determinations.

Experimental diamagnetic corrections were made for the host zeolite over the same temperature and field strength ranges.

(iv) Adsorption:

The amount of gas adsorbed by a surface is measured as a difference between two large numbers, the amount of gas originally injected into the adsorption cell under conditions where negligible gas-surface interaction takes place and the amount of gas remaining in the gas phase after equilibration over the solid sample when measureable interaction occurs.

In the design of any adsorption system therefore, it is necessary to have accurate system segment volumes, pressure measurement and temperature control in order to minimize the error in the volume of gas adsorbed.

Adsorption studies are generally made using a volumetric apparatus[19] which measures the volume of gas uptake by an adsorbent. This apparatus incorporates a dosage system and pressure measuring system, an adsorption cell, temperature control unit and pumping facilities capable of obtaining a high vacuum. The design of each of these components is governed by the range over which temperature and pressure measurements are to be made, the desired precision of the measurements and the characteristics of the materials used as adsorbate and adsorbent.

The volumetric apparatus of Figure 2 consists of: a gas purification train (A, B, C) in which impurities could be removed by trap-to-trap distillation; a pair of bulbs (D) used for the storage of gases after distillation; and finally the adsorption system enclosed within the dotted lines of Figure 2 and described in the following paragraphs.

a) Dosage System[19]

Gas was introduced to the adsorption system directly from the external storage bulbs. Five mercury pipets of volumes 10, 20, 40, 80 and 160 millilitres surrounded by an ice-mantle (E) were used to inject gas into the adsorption cell (G). The pipet volumes were known from repeated mercury weighings to an accuracy of .02%. These by different combinations give

Index For Figure 2

A	TO GAS LECTURE BOTTLES
B	DISTILLATION TRAPS
C	MERCURY MANOMETER
D	GAS STORAGE BULBS
E	ICE MANTLE AND PIPETS
F	IONIZATION GAUGE
G	ADSORPTION CELL
H	MERCURY MANOMETER
I	THREE-STAGE MERCURY DIFFUSION PUMP

FIG 2

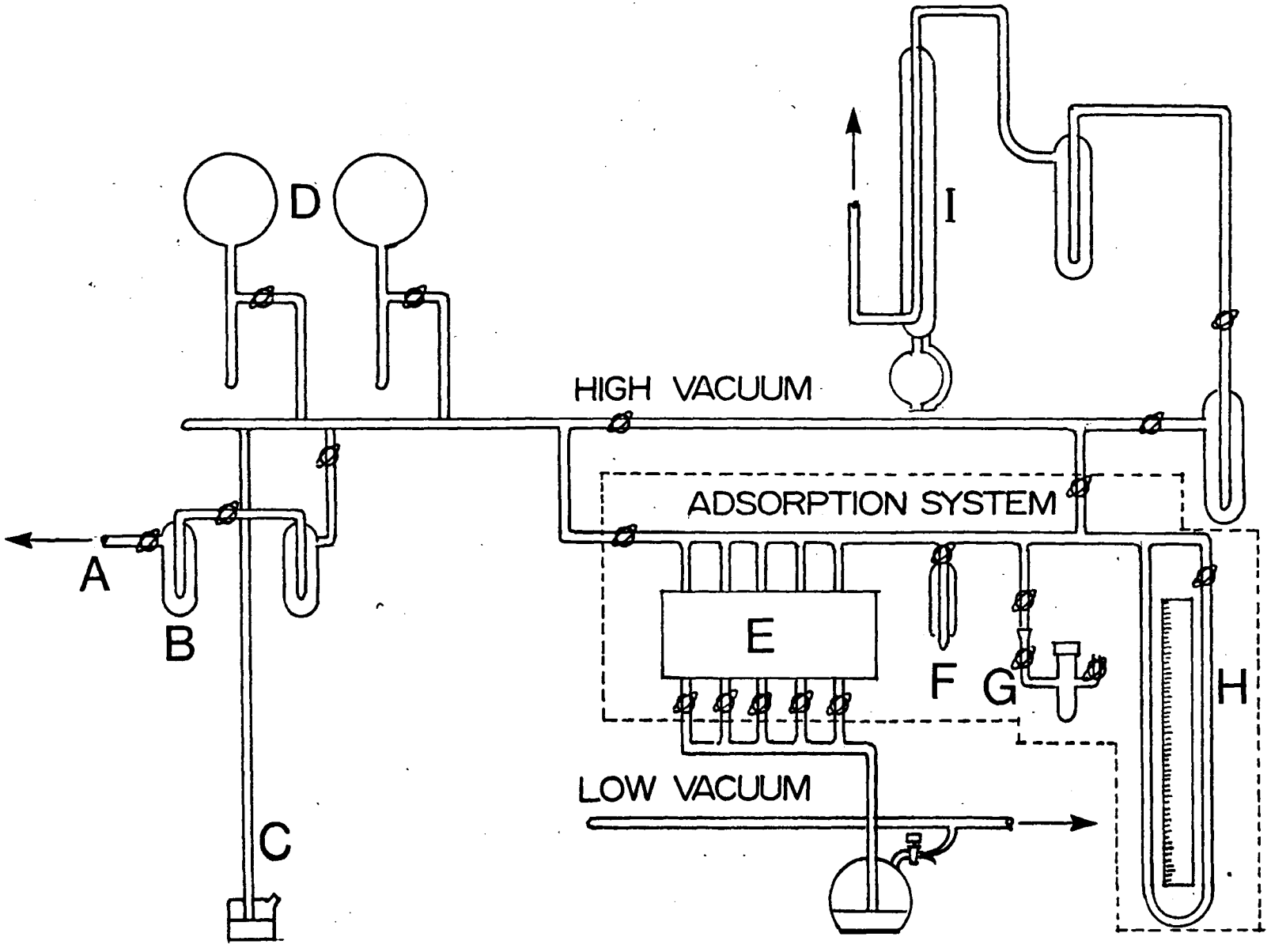

volumes of between 0 and 310 ml in 10 ml increments.

Owing to the geometry of the system, gas pressures above 450 torr could not be obtained.

At times during a run a large fraction of the gas was contained in the pipets. As the temperature control and measurement of an ice-mantle is virtually free from experimental error and the pipet volumes were known accurately, the error in the estimate of the amount of gas in the adsorption cell was essentially independent of this part of the system.

b) Pressure Measurement

The gas pressure in the system was measured with a mercury manometer (H) connected in series with the adsorption cell and pipets, and placed as close to the cell as possible in order to minimize the dead space volume. The manometer was mounted in a wooden platform against a dull white background which provided sufficient contrast to give sharp menisci under conditions of normal room illumination. Between the fixed and free legs was mounted a stainless "Starrett-steel" meter bar graduated in 0.5 mm increments which was read with the sliding microscope of a cathetometer. For low pressure readings the cathetometer (which was securely anchored to the floor to insure maximum reproducibility of readings) was used to obtain a more accurate estimate of the meter bar reading to ±0.1 mm.

Both the fixed and free legs of the manometer were constructed of 14.6 mm (inside diameter) "Tru-Bor" tubing with the object of minimizing capillary depression effects and hence of obtaining well-defined and relatively flat menisci.

c) Adsorption Cell

Figure 3 shows details of the adsorption cell. For ease of changing samples the cell was fitted with a metal screw cap made of nickel plated brass, seated on a Teflon "O" ring. This was attached to the cell by means of a Kovar seal. The use of teflon tape around the threads assured attainment of the desired vacuum even after repeated sample changes.

One of the side arms was included as part of the cell in order to measure the evacuated weight of the zeolite and subsequently to determine the sample volume from its density. The other was included to allow the passage of hydrogen over the sample when reduction experiments were conducted as described later. These side arms have the disadvantage of increasing the cell overhead volume but in terms of the total dead space volume of the system, the increase is small.

Only part of the cell was thermally controlled during adsorption measurements (the section in Figure 3 marked by the dotted line). The remaining volume was included as part of the cell overhead volume and assumed to be at room temperature. The error in the volume adsorbed created by this assumption was found to be negligibly small.

The volume of the cell was determined from repeated weighings with distilled water.

The temperature at which the isotherms were measured are: liquid nitrogen (77^{o}K), dry ice slush (195^{o}K), chloroform slush (210^{o}K) and carbon tetrachloride slush (250^{o}K). The temperature of these baths were measured with an iron-constantan thermocouple attached to the adsorption cell.

Index For Figure 3

A METAL CAP

B KOVAR SEAL

C CELL VOLUME

FIG 3

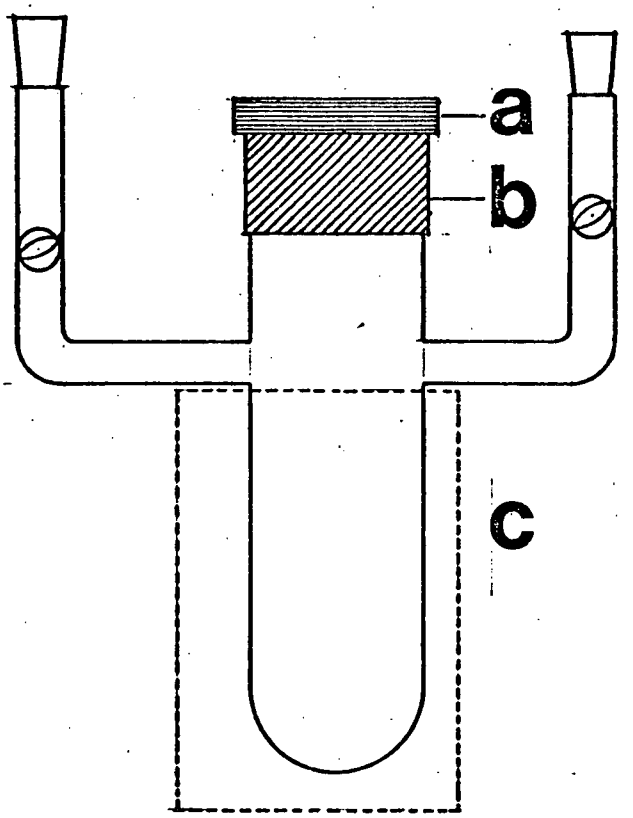

Under sample outgassing conditions (or when hydrogen was used to sweep the zeolite) a furnace was fitted round the cell, and the outgassing temperature was maintained by a previously calibrated rheostat to $\pm 5^{o}C$.

d) Associated Equipment

The pumping equipment for the high vacuum line consisted of a three-stage mercury diffusion pump (I of Figure 2) backed by a Welch rotary oil pump. This assembly was capable of obtaining a vacuum of 10^{-6} torr. The low vacuum line which served only to evacuate the mercury pipet reservoirs was also connected to a Welch rotary oil pump.

Beckman thermometers were used to measure room and ice mantle temperatures. Both were calibrated against a standard platinum resistance thermometer.

Dead Space Determination and System Error:

The overhead volumes of the pipets and cell were measured gasometrically with helium at room temperature, and are given in Table 2.

Temperature fluctuations in the slush baths and ice-mantle were negligible. Room temperature variations were no greater than 0.3^{o} for any point (P,V) on the adsorption isotherm.

The initial gas dosage pressure P_I was about 5 torr and depending upon the surface gas uptake the equilibrium pressure P_E could be as small as 0.1 torr. Since the error limits on the pressure are ±0.1 torr the lowest pressure P_E can have an error as large as 100%. However this only creates an error of 7% in the corresponding value of the volume adsorbed.

Table 2

Volume of System Segments

Pipet	Volume cc	Section	Volume cc
1	159.17±.005	cell	12.62±.01
2	79.612±.001	OH pipet	131.0±.5
3	39.419±.001	OH cell	22.3±.1
4	18.003±.001		
5	9.402±.001		

Equations (1), (2) and (6) in the Appendix show how the volume adsorbed is calculated. As an example, using

$P_I = 5 \pm 0.1$ torr

$P_E = 0.1 \pm 0.1$ torr

and the volumes listed in Table 1 the error in n_I is ±4% and in n_E is 100% but the error in n_A is only 7%. As the pressures increase so does their accuracy and consequently the error in n_A becomes smaller.

The error estimate on the volume adsorbed for the low pressure region is therefore 7%; and this decreases to approximately 2% in the region of high pressure.

Blank adsorption-isotherms (that is with the cell empty) were determined with CO_2 and C_2H_6 in order to see whether any adsorption of these gases on the remainder of the system occurred. The values obtained for both gases differed by less than 2% from those obtained with helium. Hence no appreciable system adsorption needed to be taken into account.

Over the range of temperatures and pressures studied gas-imperfection corrections were sufficiently small to be ignored. The magnitude of thermal transpiration corrections between the parts of the system at liquid nitrogen and room temperatures were also negligibly small and hence ignored.

(v) Mössbauer Apparatus:

Two types of Mössbauer cell were used in order to accommodate powder and pellet samples.

Powder samples were packed to a thickness less than 1mm

in a 1.25 cm diameter brass cell having mylar windows. For room temperature runs the cell was mounted on an aluminum holder directly in the γ-ray path. For liquid nitrogen runs the cell was inserted in the top of a copper cold-finger which was immersed in a dewar of liquid nitrogen. Styrofoam insulation was placed around the sample to minimize heat transfer and to obtain a temperature as close to 80° K as was feasible by this geometry. The nitrogen level was maintained by a Superior Air Products Company liquid nitrogen level-controller.

Figure 4 represents the cell used for pelletized samples. Previous cell designs consisted of a removeable head with rubber "O" ring and beryllium windows, neither of which permitted the cell to hold a vacuum after one or two cycles between liquid nitrogen and room temperature.

In order to make comparisons between Mössbauer and adsorption experiments the Mössbauer cell had to maintain a vacuum between room and liquid nitrogen temperatures through many temperature recyclings, and be capable of holding a given pressure of gas under the same temperature conditions. The B34 joint was substituted for the removeable head to allow sample insertion. The head was constructed from solid nickel-plated brass and the mylar windows were attached by an indium seal over which was a screw cap that distributed the seal evenly. After more than forty temperature recyclings no leaks were detected and during a given Mössbauer experiment the cell was capable of maintaining a high vacuum for several days. The side arms

FIGURE 4

Diagram of the Mössbauer Cell
used for pelletized samples

FIG 4

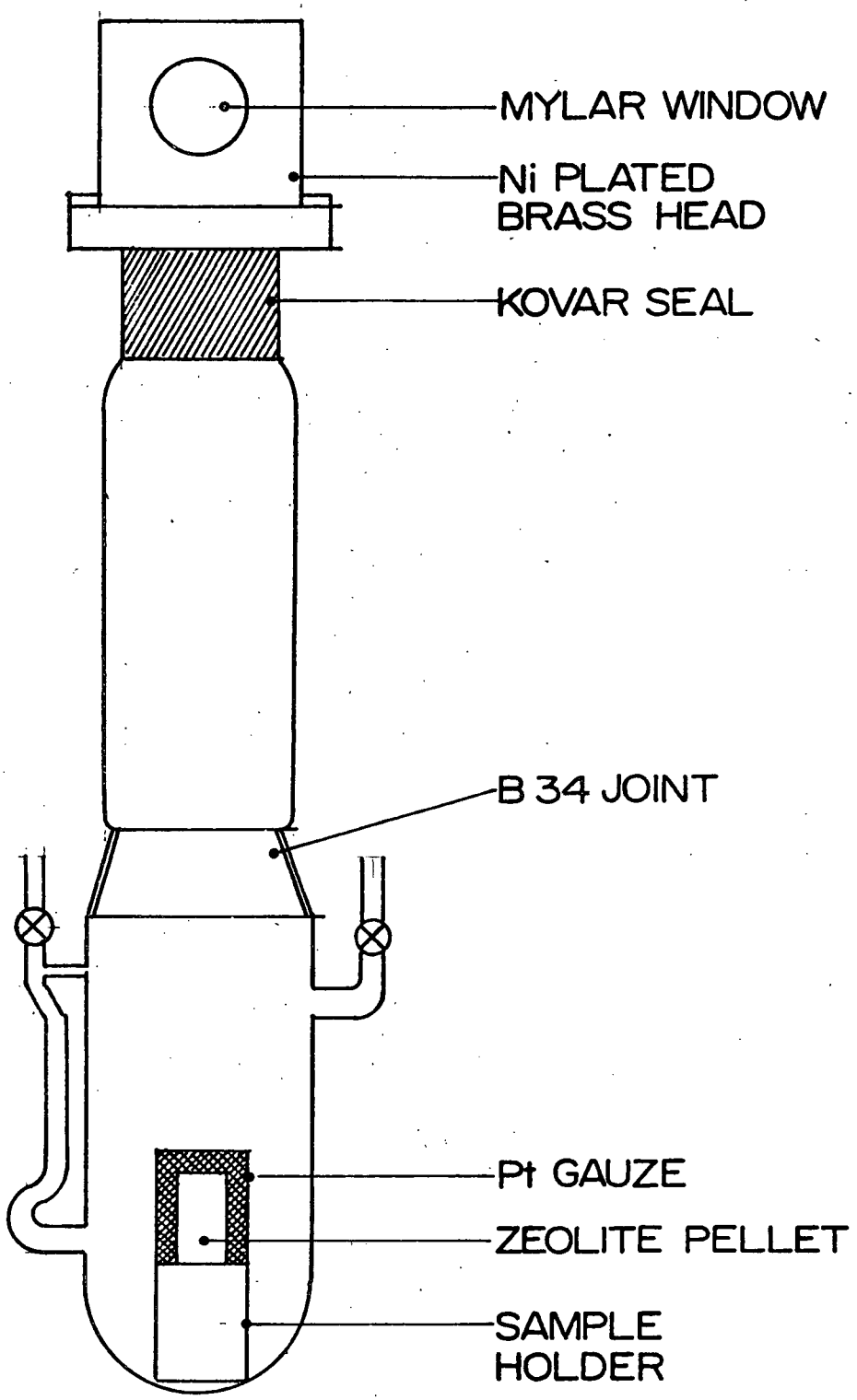
MYLAR WINDOW
Ni PLATED
BRASS HEAD
KOVAR SEAL
B 34 JOINT
Pt GAUZE
ZEOLITE PELLET
SAMPLE
HOLDER

allowed evacuation and gas "sweeping" of the zeolite.

Pellets were made from a Carver Laboratory Press Model B at pressures around 15,000 psi and were then shaped to fit the pellet holder of Figure 4. The pellet remained in the diagram position for evacuation, gas sweeping and high-temperature outgassing.

For Mössbauer measurements the cell was inverted. In this position the sample fits into a slot in the head, aligned with the windows. This cell was subjected to three temperatures: room, CO_2 slush, and liquid nitrogen. For the low temperature runs the cell assembly was bolted to a copper cold-finger and insulated with styrofoam.

One series of Mössbauer experiments was conducted on an evacuated powder sample which was positioned in a Janis model DT-6 "Varitemp" helium cryostat, fitted with a Cryogenic Research Corp. model RS-1 temperature control unit. With this device, any temperature between about 8^{o}K and room temperature could be maintained to within $\pm 0.05^{o}$. Calibrated germanium and platinum resistance thermometers were used to measure the sample temperature.

The Mössbauer Spectrometer was of the constant acceleration type and has been described in detail[20]. The γ-ray source consisted of 25 mC of ^{57}Co in a copper matrix, supplied by New England Nuclear Corp.

National Bureau of Standards certified sodium nitroprusside and iron foil were used for isomer shift and velocity scale calibrations, respectively. In most cases the data were least-squares fitted to lorentzian line shapes using a program

written by J.C. Scott. However, in several instances non-lorentzian lines were observed (owing to relaxation effects); in these cases Mössbauer parameters were estimated visually from the plotted spectra.

The errors in the measured parameters are based on the standard deviation of the computer fit and the reproducibility of the spectra.

RESULTS AND DISCUSSION:

In an earlier Mössbauer investigation of iron-exchange in zeolite L[17] the presence of two ferric species was reported. One of the species was presumed coordinated to the lattice oxygens while the other was thought to be $FeCl_3$. As the observed spectra[20] at liquid nitrogen and room temperature consisted of a quadrupole doublet the ferric nuclei had to be in almost identical environments. The present work was undertaken to find out 1) whether two ferric species coexisted in the zeolite and 2) the degree to which the zeolite surface was occupied by the occluded iron.

In preparing the present sample, two preliminary pieces of information were required before adsorption and Mössbauer studies could be conducted. The first was proof that the zeolite framework remained intact after treatment with iron chloride. The second requirement was a knowledge of the iron and chlorine content of the sample.

The results of X-ray powder photography are given in Table 3. The d-spacings are listed for the zeolite prior to any treatment, treated with iron chloride and a subsequently treated sample which will be discussed later. Comparison of these numbers with those in the literature for Zeolite L[21] shows that most of the d-spacings lie within the range of the reported values. Any discrepancies or omissions may be accounted for by the fact that the photographs were taken using a pin-hole collimator and the lines were thus rather weak and sometimes indistinct.

Table 3

d-Spacings from X-Ray Powder Photographs

Literature[21]	L-zeolite	iron-L-zeolite	Treated iron-L-zeolite	Bulk[34] α-Fe_2O_3
16.1 ± . 3	15.8	15.7	15.7	
				7.96
7.52 ± .04	7.49	7.43	7.37	
6.00 ± .02	5.98	5.98		
		5.90	5.90	5.86
				5.43
				4.77
4.57 ± .03	4.62	4.62		
			4.52	
4.35 ± .04	4.35	4.35	4.33	
3.91 ± .02	3.93	3.93	3.86	
	3.67	3.64	3.62	
3.47 ± .02	3.48	3.48	3.44	
3.28 ± .02	3.23		3.25	
3.17 ± .01	3.18	3.18	3.14	
3.07 ± .01	3.08	3.06	3.04	
2.91 ± .01	2.92	2.92	2.88	
2.65 ± .01	2.66	2.66	2.65	
	2.63	2.64	2.60	
2.46 ± .01	2.48		2.48	
2.42 ± .01	2.42			
2.19 ± .01	2.20	2.20	2.17	

The chemical analysis performed on the sample (Table 1 - #3) shows that both iron and chlorine are present in the approximate mole ratio of 2:1, and that the silicon-to-aluminum mole ratio of approximately 3:1 for zeolite L[22] is preserved. Also listed in Table 1 (#1 and #2) are the carbon contents for untreated and solvated zeolite L. The very small percent increase in the solvated sample is not indicative of any appreciable ether-surface complex formation.

These results indicate that both iron and chlorine entered the zeolite without disrupting the lattice.

The Mössbauer spectrum of a powdered sample of iron-L-zeolite in air showed a quadrupole doublet. The isomer shift was characteristic of high spin ferric compounds (typical values for Fe^{3+} are $\delta \approx 0.6$ mm/sec, whereas for Fe^{2+} $\delta \approx 1.2$ mm/sec and Fe° $\delta \approx 0.26$ mm/sec). At liquid nitrogen temperatures however, additional very broad lines indicative of Zeeman splitting were observed. The magnitude of the internal magnetic field (approximately 400 kOe) was considerably less than the field strengths normally observed for five unpaired electrons. (The theoretical contribution to the field is about 110 kOe per unpaired electron, but due to the interactions between an ion and its surroundings this value is usually slightly quenched. Typical observed fields are approximately 510 ± 20 kOe).

The presence of a doublet at room temperature and a hyperfine pattern superimposed on the doublet at liquid nitrogen temperatures seemed to be typical behaviour attributable to relaxation effects. The very broad nature of

the outer lines and the extremely low value of the internal field strength suggested that at lower temperatures the lines may become better resolved as the internal field increased towards its saturation value. Figure 5 shows the behaviour of the sample between 295^{o}K and 9^{o}K and Table 4 lists the Mössbauer parameters extracted from these spectra.

The 80^{o} and 9^{o}K parameters were obtained from the "Varitemp" helium cryostat. The remaining temperature runs were made using the Mössbauer cell and the appropriate coolant as described earlier. Figure 5 does not include the spectra corresponding to the 80^{o}K parameter in Table 4. However the difference between this spectrum and Figure 5c) was quite apparent. While the doublet still remained, the outer lines were more intense and better resolved.

The liquid nitrogen temperature parameter for the powder and pellet samples are recorded in the table as approximately 105^{o}K. Several spectra between 80^{o} and 120^{o}K were obtained at known temperatures in the helium cryostat. The approximate temperature range in which Figure 5c) fit was 100^{o} - 110^{o}K and hence the average value of 105^{o}± 5^{o}K was chosen.

Also included in Table 4 is a comparison of the Mössbauer parameters between pelletized and powdered samples. As can be seen from their isomer shifts and quadrupole splittings in air the two sample preparations have identical values. Thus the same trends are expected in both over the temperature range studied. (Figure 7a) to be discussed later represents a powder sample in air at approximately 105^{o}K which could be compared with Figure 5c)).

FIGURE 5

Mössbauer Spectra of

a) pellet in a vacuum at 295°K

b) pellet in a vacuum at 195°K

c) pellet in a vacuum at ∿105°K

d) powder in a vacuum at 9°K

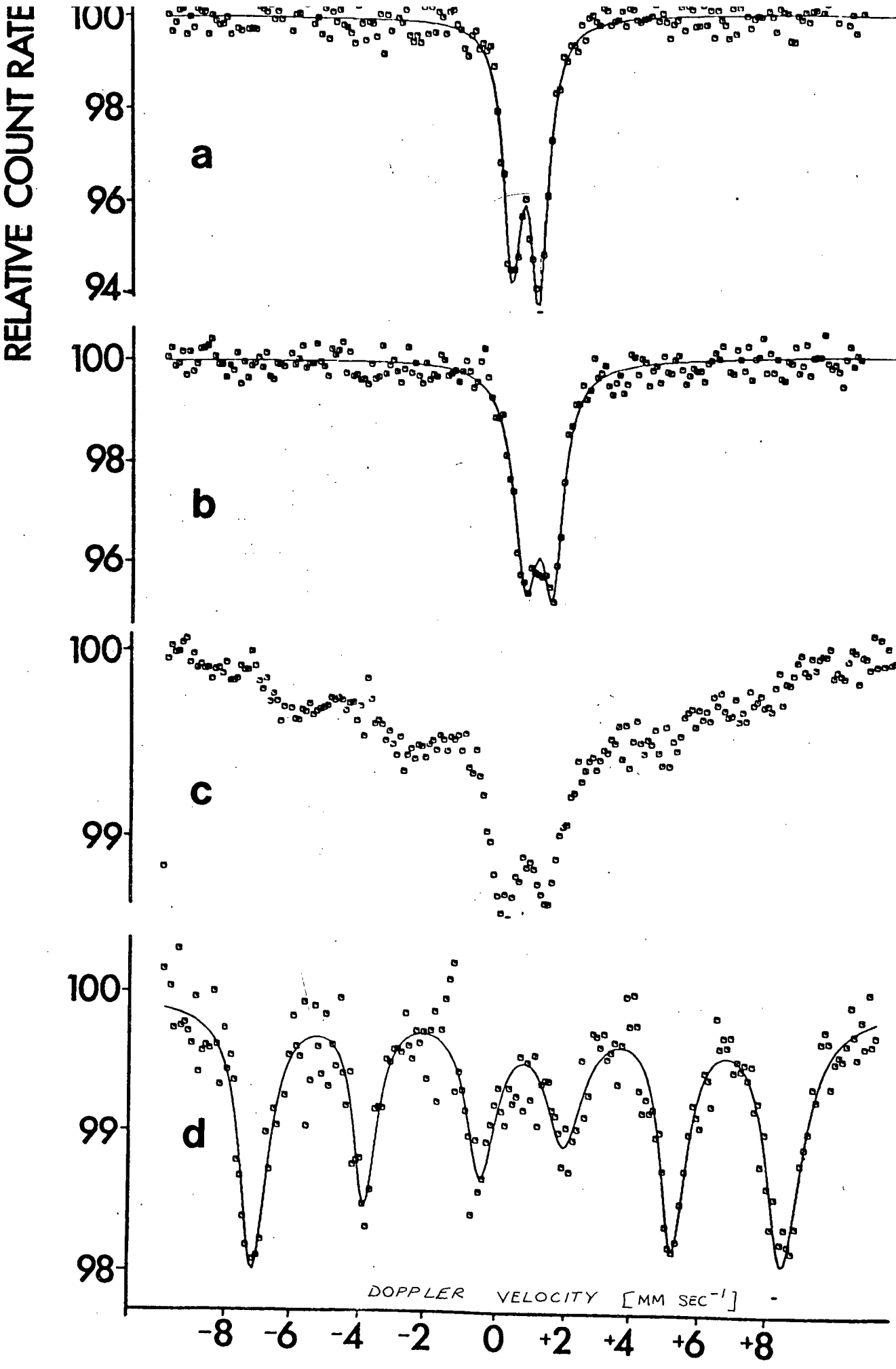
RELATIVE COUNT RATE
100
98
96
94
a
100
98
96
b
100
99
c
100
99
98
d
DOPPLER VELOCITY [MM SEC⁻¹]
-8 -6 -4 -2 0 +2 +4 +6 +8

FIG 5

Table 4*

Sample	Temp (°K)	δ[a]	Δ[a]	Γ[a]	H[b]
1) pellet in air, no treatment	295	0.64 ± .02	0.73 ± .02	0.68 ± .02	-
	∿105	0.75 ± .04	0.96 ± .02	1.1 ± .1	402 ± 25
in vacuum	295	0.63 ± .02	0.79 ± .02	0.59 ± .02	-
	195	0.6 ± .1	0.75 ± .02	0.74 ± .02	-
	∿105	0.69 ± .02	1.2 ± .05	1.2 ± .1	402 ± 25
2) powder in vacuum	80	0.60 ± .04			430 ± 20
	9	0.65 ± .04	∿0		467 ± 20
3) powder in air					
a) no treatment	295	0.63 ± .02	0.76 ± .02	0.60 ± .02	-
	∿105	0.76 ± .04	1.00 ± .05	1.6 ± .1	402 ± 25
b) calcined at 573°K in air	295	0.63 ± .02	0.98 ± .02		-
c) calcined at 773°K in air	295	0.73 ± .02			514 ± 20
	∿105	0.62 ± .05			501 ± 30
4) [c]Bulk α-Fe_2O_3	298	0.62			516

Continued/.....

Table 4* Continued

Sample	Temp (°K)	δ[a]	Δ[a]	Γ[a]	H[b]
5) Powder washed with hot water	295	0.64 ± .03	0.78 ± .02	0.52 ± .04	-
	∿105	0.70 ± .02	1.1 ± .1	1.5 ± .2	d

[a] in mm/sec relative to sodium nitroprusside

[b] in kOe

[c] Reference #6

[d] outer lines not resolved

* data was obtained from simple plots of spectra at ∿105°K

The most apparent features of the spectra of Figure 5c) are the following:

1) The Zeeman splitting observed at 105°K completely collapses at 195°K. 2) The broad outer lines at 105°K are much better resolved at 9°K where the size of the internal magnetic field has obviously increased (represented by an increase in the splitting between lines one and six). 3) The central doublet has virtually vanished at 9°K. 4) The six-line pattern at 105°K is superimposed on a parabolic base-line and the line-shapes are non-lorentzian (this is also true of the 80°K spectrum).

Since one of the probable coordinations of a ferric ion in this zeolite is to lattice oxygens, the above evidence pointed to small particle iron oxide behaviour. Constabaris, Kündig and co-workers[23,24] have examined by Mössbauer spectroscopy the properties of small particles of α-Fe_2O_3 supported in silica gel, as a function of temperature and particle size. Their results are now discussed as they apply to the present work.

First, for a given average particle size of α-Fe_2O_3 in the support, the temperature dependence shows a doublet at 295°K and a six-line pattern superimposed on the doublet at 80°K. But the line shapes of the hyperfine pattern are lorentzian and the observed splittings between lines one and six differ very little between 80° and 12°K. Second, the intensity ratios of the magnetic hyperfine lines are always approximately the same (1:2:3); and are characteristic of the transition probabilities in the magnetic spectrum of

bulk α-Fe_2O_3.

Small particles of α-Fe_2O_3 exhibit superparamagnetism. The effect is observed by Mössbauer Spectroscopy as the collapse of a six-line spectrum into a doublet. The transition occurs at a specific temperature for a given particle size and represents the difference between magnetic order (anti-ferromagnetic behaviour in α-Fe_2O_3) and magnetic disorder (paramagnetic behaviour) respectively. The size of the internal magnetic field generated by magnetic ordering for a given particle size differs very little from that of bulk α-Fe_2O_3. As these effects are the result of particle relaxation times, the above behaviour is specific for a given particle size with a given relaxation time.

However where a distribution of relaxation times is exhibited in a sample a) the transition temperature between magnetic order and disorder varies over a range of temperatures b) the line shapes of the hyperfine pattern are usually non-lorentzian and c) the magnitude of the internal magnetic field varies over a wide range of temperatures.

The behaviour pattern of the spectra in Figure 5 is sufficiently different from the superparamagnetic behaviour of an average particle size of α-Fe_2O_3 that the latter can be ruled out on the Mössbauer evidence alone. However, as spin relaxation effects occur in simple paramagets as well as magnetically ordered paramagnets, measurement of the temperature and magnetic field dependence of the molar susceptibility should distinguish between the two.

Figure 6 shows the molar susceptibility of iron in

FIGURE 6

Magnetic Measurements on iron-L-zeolite

a) Molar susceptibility of iron versus temperature

b) Effective magnetic moment versus temperature

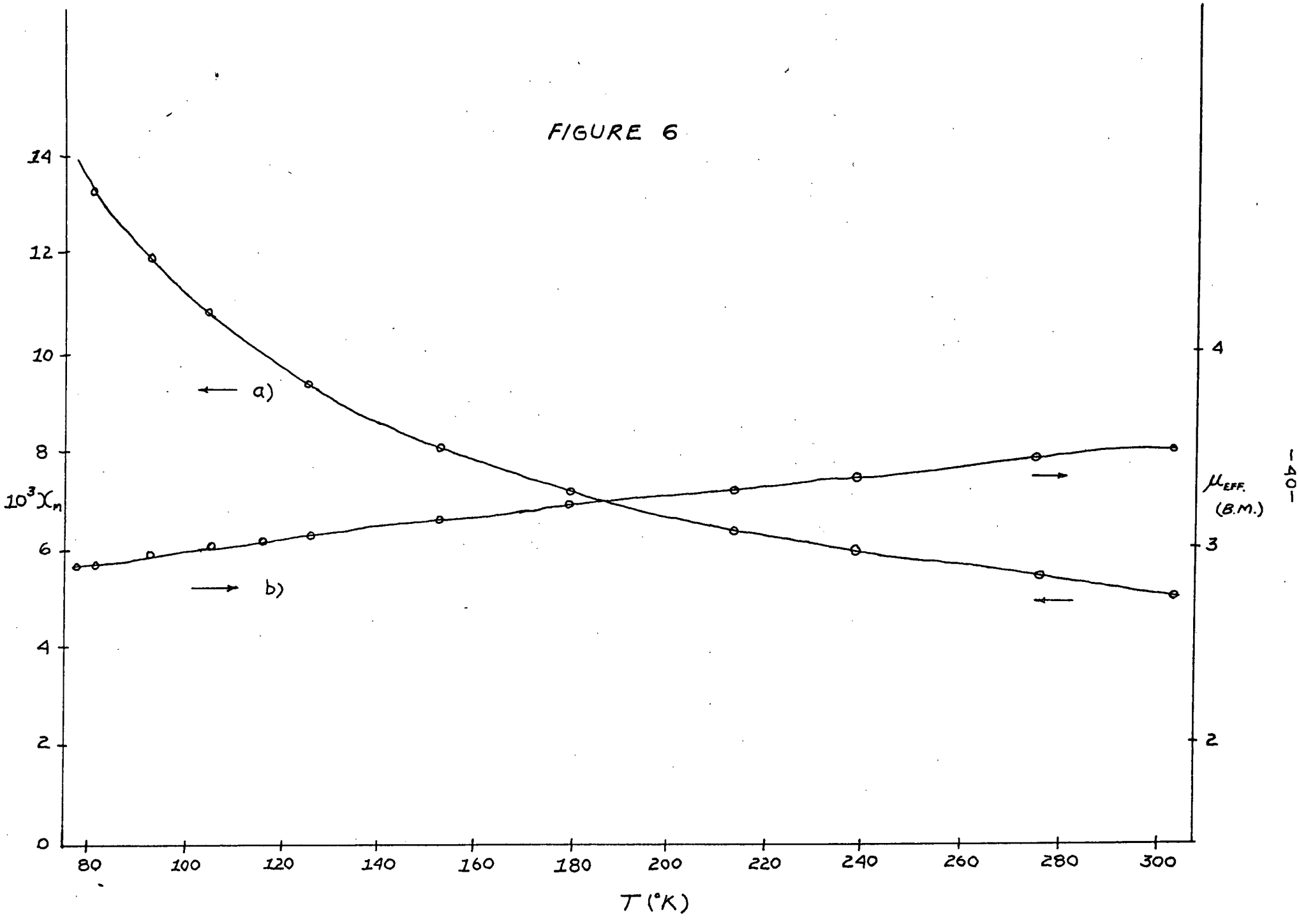
FIGURE 6
14
12
10
8
6
4
2
0
$10^3 \chi_m$
a)
b)
4
3
2
$\mu_{EFF.}$
(B.M.)
80
100
120
140
160
180
200
220
240
260
280
300
T (°K)

zeolite L as a function of temperature and field strength. No dependence on an externally applied magnetic field was observed, as the susceptibilities at three applied fields all lie on the same temperature curve. Hence at least down to 80°K the sample behaves like a simple relaxing paramagnet.

The variation of the effective magnetic moment (μ_{eff}) is also plotted as a function of temperature in Figure 6. The surprisingly low moments and their variation with temperature (3.4 - 2.9 B.M. between 300° and 80°K) is not the typical behaviour of a simple paramagnetic ferric compound. However low magnetic moments (2.3 - 5.9 B.M.) in ferric compounds[25] have been attributed to 1) spin exchange interactions between ion-ion and ion-ligand and 2) the presence of magnetically non-equivalent sites in a lattice. In the latter effect Curie-Weiss behaviour is still observed. Below 160°K Curie-Weiss behaviour was also exhibited by the present sample. Either of these effects, however could account for the present results.

Although the sample appears to behave like a simple paramagnet down to 80°K, field dependence studies at temperatures lower than this are required in order to categorically state that the ferric species of Figure 5 is a simple paramagnet.

Two further pieces of information can be obtained from Table 4 and Figure 5. The disappearance of the parabolic base-line and appearance of a lorentzian six-line spectrum at 9°K are definite indications of magnetic ordering with long spin-lattice relaxation times. The inner doublet does not appear to have completely vanished which could be the

reason for the slightly broadened nature of the lines in the spectrum. However, the trend that is observed in the disappearance of the central doublet and an approach toward a maximum internal field strength with decreasing temperature (if indeed the maximum has not already been reached) is indicative of a single ferric species within the sample. This does not preclude the possibility of more than one ferric site within the sample whose geometries may be sufficiently similar that Mössbauer resolution would be impossible.

The range of temperature over which the relaxation effects occur (approximately 40^{o}) strongly suggest that different parts of the system relax at different rates. Correlations have been made between particle size and relaxation time[26]; and it is known that as the particle size is decreased the relaxation time becomes shorter. Hence the sample may contain a range of particle sizes. Alternatively this may simply be a function of the distance between iron centres. As will be discussed later, the measured decrease in surface area between solvated L-zeolite and iron-L-zeolite shows definitely that the pores are blocked by the ferric species. This, coupled with the very low magnetic moments obtained from magnetic measurements tends to rule out particle size variation.

The presence of chloride ion from chemical analysis could imply that ferric chloride was in the sample. In order to show that the observed Mössbauer spectra were not the result of relaxation effects in ferric chloride an additional experiment was performed. A sample was washed with hot water

and the filtrate was tested for chloride and ferric ions. A very positive test with silver nitrate resulted for the chloride ion but with KCNS only trace amounts of the ferric ion could be detected. Washing continued until no further evidence for either ion was evident. A comparison of the room and liquid nitrogen temperature Mössbauer parameters for the washed sample with those of the original untreated sample (Table 4) show that there is no change in the parameters. Neither is there any appreciable alteration of the Mössbauer spectrum.

The very positive nature of the chloride ion test indicated that a large percentage of it had been removed from the zeolite. The almost negative test for ferric ion indicated that ferric chloride was not being washed out as a species. Also if ferric chloride existed in the sample in the amount suspected by chemical analysis, washing it out would have markedly changed the Mössbauer per cent effect. This also did not happen. However, ferric chloride may be present as an impurity but as a sufficiently small percentage of the overall ferric content that it is not observeable by Mössbauer Spectroscopy. The bulk of the chloride ion may be present as a sodium or potassium chloride. Having eliminated fine particle α-Fe_2O_3 and possibly $FeCl_3$ as sources of the Mössbauer spectra and considering the evidence for a single ferric species occluded in the zeolite, one other possibility consistent with ferric coordination to lattice oxygens would be an oxy-hydroxide of iron.

The bulk behaviour of different types of iron-oxyhydroxides

have been studied by many authors[27-30]. Dezsi[30] and co-workers have looked in particular at the bulk behaviour of β-FeOOH. Relaxation effects in β-FeOOH were followed by Mössbauer Spectroscopy from 120°K to 295°K. The relaxing six-line spectra showed a parabolic base-line. The outer lines were very broad and there was no definite ratio of the outer to inner line intensities. The Neel point (the temperature at which the transition occurs from paramagnetic to ordered magnetic behaviour) was found to be 295°K and the saturation magnetic field at zero temperature was 475 kOe. Of further interest were the spectra obtained on the sample at different temperatures of calcination in air. The Mössbauer Spectra consisted of a high spin ferric doublet between 295° and 670°K. Above this temperature a transition occurred and the six-line hyperfine pattern of α-Fe_2O_3 developed. Similar behaviour is observed in δ-FeOOH[30].

Table 4 and Figure 7 show the results of calcining the iron-L-zeolite sample in air. After heating in air at 573°K the room temperature spectrum is a doublet and the liquid nitrogen temperature spectrum is a non-lorentzian six-line pattern. The quadrupole splitting of the room temperature doublet has increased from that of the untreated sample, which is consistent with the removal of water molecules from the ferric coordination sphere. Finally after heating at 773°K the spectrum of Figure 7b) is obtained. For comparison the parameters of bulk α-Fe_2O_3 are listed in the table.

Although this is by no means conclusive evidence for a

FIGURE 7

Room temperature Mossbauer spectra of powder calcined in air

a) untreated powder sample

b) powder sample calcined at 773^{o}K

FIG 7

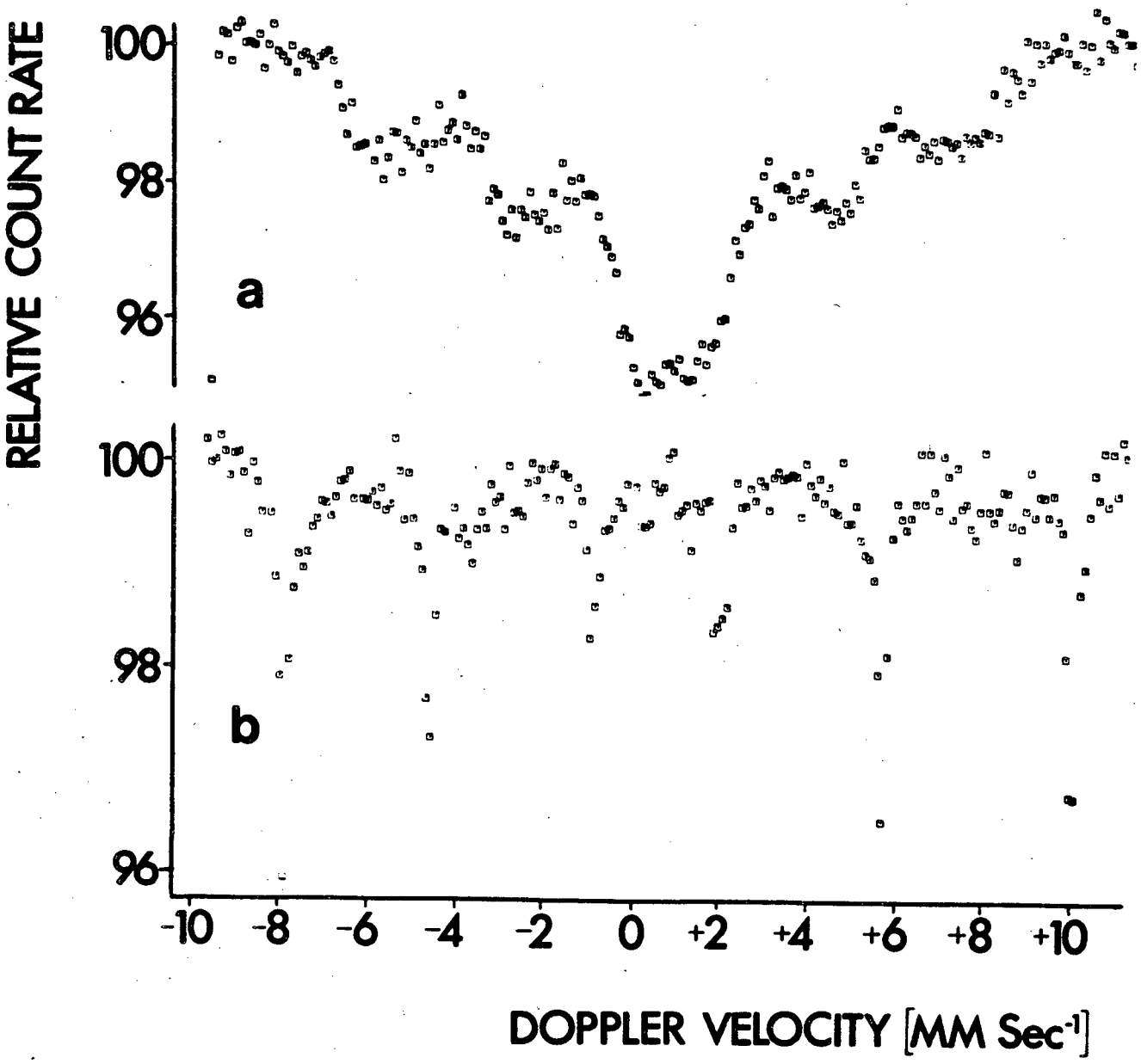
RELATIVE COUNT RATE
100
98
96
a
100
98
96
b
-10
-8
-6
-4
-2
0
+2
+4
+6
+8
+10
DOPPLER VELOCITY [MM Sec-1]

change between oxy-hydroxide and α-Fe_2O_3 in the present sample it is certainly not negative evidence. Recent evidence has been reported for the presence of small particle α-FeOOH in natrolite which goes to α-Fe_2O_3 when calcined in air[31]. The room temperature spectrum of Figure 7b) is also a six-line hyperfine pattern.

The evidence reported then for this sample of iron-L-zeolite suggests that only one ferric species is present and that this species may occupy more than one type of geometry within the zeolite lattice. The sample exhibits simple paramagnetic behaviour down to 80^{o}K (magnetic measurements) and with only the Mössbauer evidence this may continue down to 9^{o}K. If lower temperatures were studied by Mössbauer Spectroscopy extrapolations could be made to determine the magnitude of the internal magnetic field at 0^{o}K. This would not necessarily identify the ferric ion bonding (there are many compounds of iron whose internal magnetic fields are very similar) but would be conclusive evidence for the presence of only one ferric species.

If magnetic measurements were to be conducted at lower temperatures the state of magnetic order or disorder could be shown between 80^{o} and 4^{o}K. If the relaxation effects observed are the result of varying distances between iron nucleii such an experiment would certainly support it. Lowering of the bulk property Neel temperature is known to accompany small particle behaviour[6]. This type of evidence would lend itself to identifying the ferric species.

However, in the absence of any more definitive information,

the ferric species within the zeolite appears to behave like an iron oxyhydroxide. The presence of hydroxyl groups on the lattice framework of zeolites is well known and certainly is consistent with ferric oxyhydroxide formation. If the internal field at $9^{o}K$ (468 kOe) is a good approximation to the $0^{o}K$ field then small particle β-FeOOH may be the iron species present here.

Mössbauer Spectra were used to determine the effects on the ferric ion created by the following sample treatments 1) room temperature outgassing and subsequent adsorption of nitrogen, carbon dioxide and ethane 2) outgassing in a vacuum at $573^{o}K$ followed by adsorption of the same gases and 3) passing hydrogen over the sample at different temperatures.

1) Table 5 lists the Mössbauer parameters for the room temperature evacuation of the sample and subsequent adsorption of gases.

The differences in the Mössbauer parameters between the pellet in air and the room temperature evacuated pellet lie primarily within the experimental errors in the data. Hence the evacuation process has not noticeably affected the coordination about the ferric ion.

The differences between the room temperature and $105^{o}K$ parameters are registered as an increase in the magnitude of the quadrupole splitting and a broadening of the line-width of the central doublet. Hence the EFG at the ferric ion is smaller at 295^{o} than at $105^{o}K$. The cause could be a result of the thermal energy available at room temperature. As the temperature is lowered inhomogeneities in the environment

Table 5*

Treatment of pellet	Temp (°K)	δ^a	Δ^a	Γ^a	H^b
evacuated	295	0.63 ± .02	0.79 ± .02	0.59 ± .02	-
	195	0.6 ± .1	0.75 ± .02	0.74 ± .02	-
	∿105	0.69 ± .02	1.2 ± .05	1.2 ± .1	402 ± 25
440 torr N_2	295	0.66 ± .02	0.75 ± .02	0.50 ± .02	-
	∿105	0.6 ± .05	1.1 ± .05	1.2 ± .1	c
reevacuated	295	0.6 ± .05	0.73 ± .02	0.7 ± .05	-
	∿105	0.66 ± .04	1.0 ± .05	1.0 ± .1	c
440 torr CO_2	295	0.6 ± .05	0.76 ± .02	0.68 ± .02	-
	195	0.71 ± .02	0.76 ± .02	0.61 ± .04	-
reevacuated	295	0.64 ± .04	0.71 ± .04	0.45 ± .05	-
	∿105	0.70 ± .02	0.86 ± .02	0.85 ± .05	c
440 torr C_2H_6	295	0.64 ± .02	0.75 ± .02	0.52 ± .02	-
	195	0.69 ± .02	0.76 ± .02	0.55 ± .03	-

Continued/.....

Table 5* Continued

Treatment of pellet	Temp (^{o}K)	δ^{a}	Δ^{a}	Γ^{a}	H^{b}
reevacuated	295	0.55 ± .05	0.66 ± .03	0.55 ± .05	-
	∿105	0.60 ± .05	0.90 ± .02	1.1 ± .05	c

* all data from ∿105 ^{o}K spectra were taken from simple plots

a in mm/sec relative to sodium nitroprusside

b in kOe

c outer lines very weak or not resolved

about the ferric ion would become more apparent as the system was "frozen down" and hence the EFG would increase. Line broadening is attributed to the changes in relaxation processes with temperature.

The gas pressures admitted to the Mössbauer cell were chosen to correspond to the maximum gas pressure studied on the adsorption isotherms (to be discussed later). After each gas was adsorbed and a Mössbauer spectrum taken the gas was removed and a spectrum was taken again to insure that the initial Mössbauer parameters remained the same.

As can be seen from Table 5, the Mössbauer parameters for the ferric ion are not significantly changed by the presence of any of the gases and hence these gases are not directly involved with the coordination sphere of the iron. Nor was there observed any change in the parameters with different gas pressures over the pellet.

Figure 8 shows the effect on the hyperfine lines of the Mössbauer spectra after gas adsorption and desorption. As is apparent from a) to c) the outer lines get weaker and are eventually unresolved. However the parabolic background still remains.

A study of the effect of the degree of hydration on the hyperfine structure of ferric ions on a sulfonate type resin has been conducted by Goldanskii et al[32]. Their findings showed that at successive stages of dehydration the magnetic hyperfine lines became weaker and eventually unresolved as the dehydration was completed. These results were explained by spin-lattice relaxation effects.

FIGURE 8

Mössbauer spectra of pellet at $\sim 105^{o}$ K showing change in hyperfine pattern with gas treatment

a) pellet in air

b) pellet in 440 torr N_2

c) pellet in vacuum

FIG 8

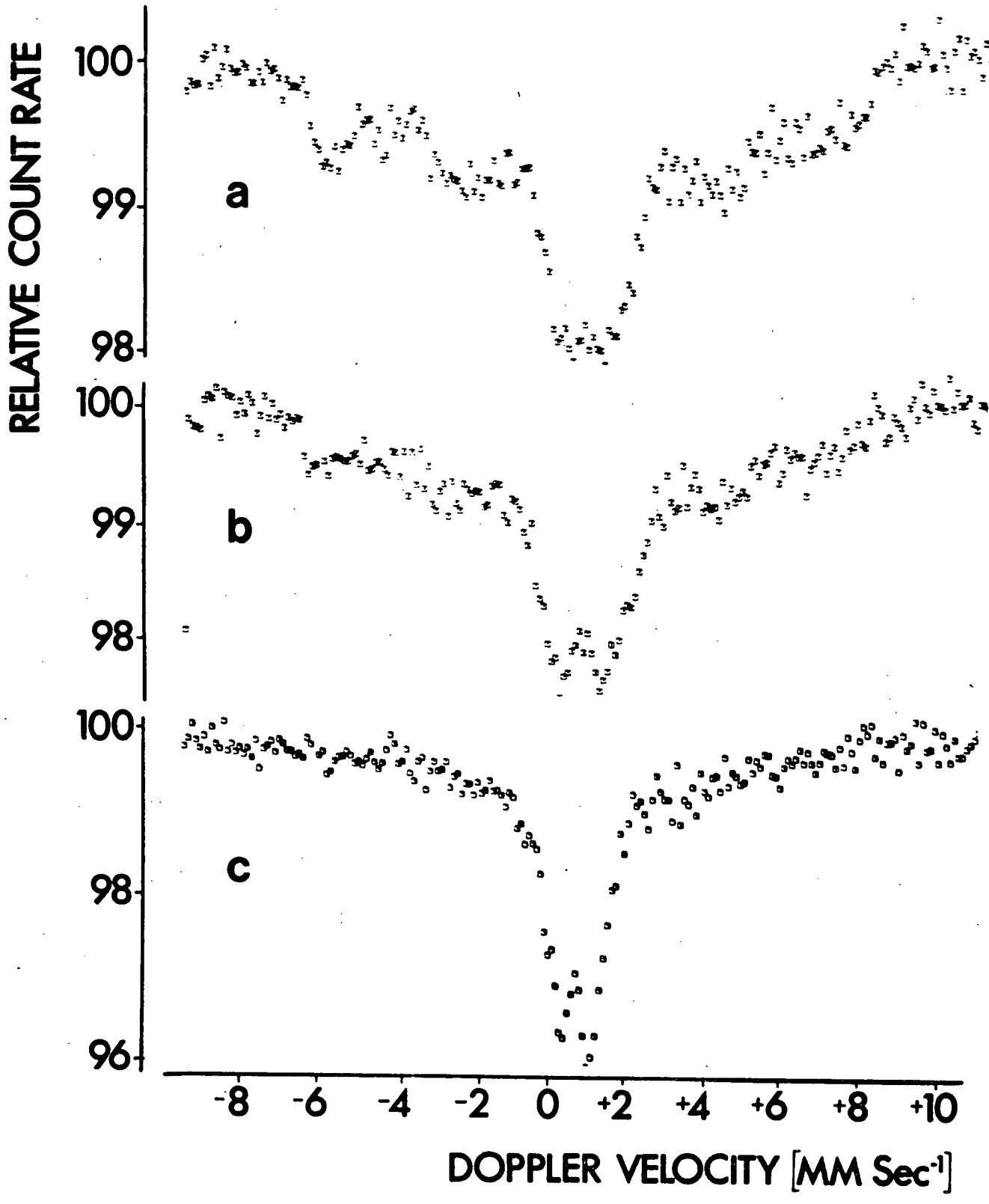
RELATIVE COUNT RATE
100
99
98
a
100
99
98
b
100
98
96
c
-8
-6
-4
-2
0
+2
+4
+6
+8
+10
DOPPLER VELOCITY [MM Sec-1]

As the various gases are introduced and withdrawn from the pellet excess water molecules within the ferric ion coordination sphere could quite conceivably be removed. The use of gases to "clean" impurities from surfaces is a well known technique. Presumably the presence of excess water around the ferric ion would increase the distance between ferric ion centres and consequently increase the relaxation time. At this point a magnetic hyperfine pattern would result. Withdrawal of the extra water then causes the reverse effect and the hyperfine pattern becomes unresolved.

On a previously made pellet of the same sample exposure to air at this point resulted in a spectra similar to that of Figure 8c). Hence the extra water molecules probably are the result of the method of preparation of iron-L-zeolite and cannot be re-introduced into the ferric ion coordination sphere by exposure to air or water washing. (Figure 8c) is essentially identical to the spectrum obtained for the washed powder sample of Table 4).

2) Table 6 lists the Mössbauer parameters for the 573^{o}K outgassed pellet and the results after various pellet treatments. The increase in the magnitude of the quadrupole splitting at 295^{o}K from that of the evacuated pellet of Table 5 to that of the outgassed pellet of Table 6 is probably the result of decreased symmetry about the ferric ion caused by the removal of water from its coordination sphere. This of course would result in an increase of the EFG at the ferric nucleus. A similar increase was also observed for the powder sample of (Table 4) after it had been calcined in air at 573^{o}K.

Table 6*

Pellet Treatment	Temp (^{o}K)	δ^{a}	Δ^{a}	Γ^{a}	H^{b}
outgassed at 573^{o}K	295	0.61 ± .02	1.00 ± .02	0.64 ± .02	-
	195	0.66 ± .02	1.07 ± .02	0.9 ± .1	-
	∿105	0.5 ± .1	1.0 ± .1	c	d
in 440 torr N_2	295	0.61 ± .02	0.97 ± .02	0.85 ± .05	-
	∿105	0.72 ± .02	1.4 ± .1	c	d
reevacuated	295	0.59 ± .02	0.94 ± .02	0.62 ± .05	
	∿105	0.60 ± .05	1.2 ± .1	c	d
in 440 torr CO_2	295	0.60 ± .08	0.91 ± .02	0.68 ± .02	-
	195	0.65 ± .02	1.08 ± .02	0.80 ± .02	-
in 440 torr C_2H_6	295	0.60 ± .02	0.85 ± .05	0.64 ± .04	-
	195	0.63 ± .02	1.05 ± .02	0.90 ± .04	
reevacuated	295	0.61 ± .05	0.92 ± .02	0.57 ± .05	
	∿105	0.61 ± .05	1.1 ± .1	c	d

Continued/.....

Table 6* Continued

* The data for spectra at ∿105°K are obtained from simple plots

[a] in mm/sec relative to sodium nitroprusside

[b] in kOe

[c] asymmetric doublet

[d] outer lines very weak or not resolved

The local environment about the ferric ion remained the same between 295° and 105°K as can be seen from the similar values of Δ. The isomer shift was essentially constant and independent of outgassing temperature.

The room temperature Mössbauer Spectrum of the outgassed pellet was a symmetric quadrupole split doublet. At 105°K the non-lorentzian line-shapes of the doublet were again apparent but the outer magnetic hyperfine lines were generally not visible. The doublet at this temperature showed a slight asymmetry which became very pronounced when 440 torr of nitrogen was introduced over the pellet. The outer magnetic lines became slightly more visible. Presumably the nitrogen influences the coordination about the ferric ion by inducing some local bond-distortions and consequently causing slight alterations in the relaxation times of the system. The influence on the ferric environment can be inferred from the increase in the magnitude of Δ.

Neither carbon dioxide nor ethane caused any significant changes in the spectra.

The only oxidation state of iron to appear even after outgassing at 573°K is Fe^{3+}. There is no evidence for the appearance of Fe^{2+} which is contrary to an earlier report on a similar system[17]. However, as many authors have indicated the presence or absence of Fe^{2+} depends on the method by which an iron compound is introduced into the zeolite.

3) In an earlier investigation of iron-L-zeolite[17] the passage of hydrogen over the sample at 573°K and subsequent outgassing in a vacuum at the same temperature produced an

iron oxide. In an attempt to find out something about the mechanism for oxide formation hydrogen was passed over the present sample at different temperatures.

Figure 9a) is a room temperature spectrum of the outgassed pellet before any treatment with hydrogen. Figure 9b) is a spectrum of the pellet after 20 hours of hydrogen flow at 573^{o}K and Figure 9c) is obtained from outgassing the sample at 573^{o}K after previous treatment with hydrogen. Table 7 lists the parameters derived from these spectra.

The spectrum of Figure 9c) consists of a hyperfine six-line pattern with very broad outer lines, an asymmetric doublet, and an extra component represented by line 5 (the line numbering starts from the left of the spectrum). The central area of the spectrum is quite complicated as it contains the inner two absorption lines belonging to the hyperfine pattern, and these probably contribute to the apparent asymmetry of the central doublet. The origin of line 5 is not clear at this point.

Outgassing at 573^{o}K in a vacuum produces a well resolved six-line hyperfine spectrum superimposed on a central doublet. The isomer shift of the doublet (0.62 mm/sec) and the magnitude of the quadrupole splitting (0.83 mm/sec) are similar to those of Figure 9a). The Mössbauer parameters for the hyperfine spectrum at room and liquid nitrogen temperatures (not listed in Table 7) are characteristic of the bulk parameters of α-Fe_2O_3.

By simply outgassing a sample of iron-L-zeolite the hyperfine pattern attributed to the formation of α-Fe_2O_3 is not observed

FIGURE 9

Room Temperature Mossbauer Spectra of:

a) outgassed pellet in vacuum

b) pellet swept by hydrogen for 20 hours at 573°K

c) after hydrogen treatment pellet outgassed at 573°K

FIG 9

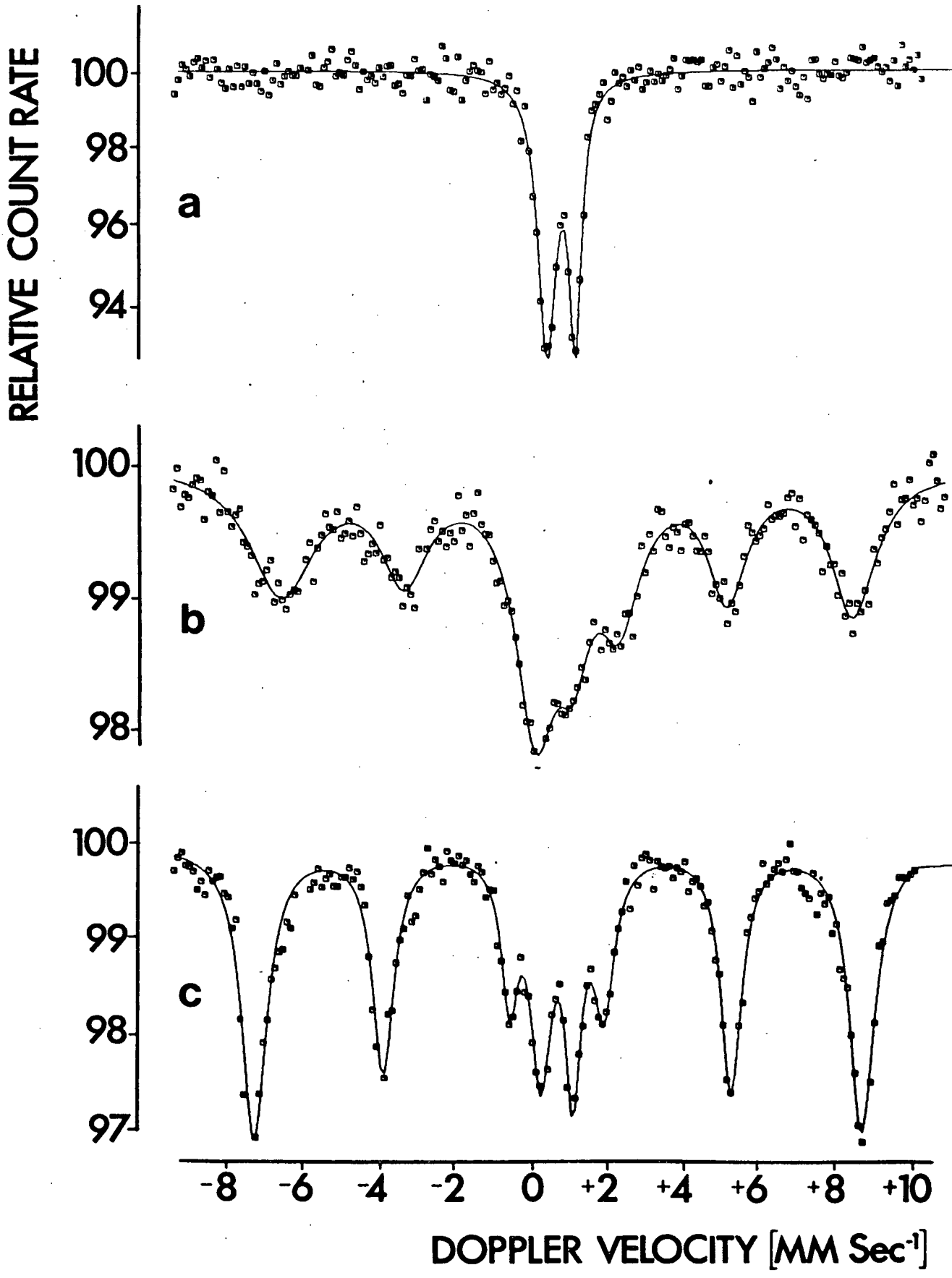
RELATIVE COUNT RATE
100
98
96
94
a
100
99
98
b
100
99
98
97
c
-8
-6
-4
-2
0
+2
+4
+6
+8
+10
DOPPLER VELOCITY [MM Sec⁻¹]

Table 7

Pellet Treatment	δ[a]	Δ[a]	H[b]	
1) after sweeping for 20 hours with H_2 at 573°K			458 ± 20	c
	1.10 ± .02	2.10 ± .02		d
2) pellet outgassed at 573°K	0.62 ± .02	0.83 ± .02		e
	0.59 ± .02	∿0	495 ± 20	c
3) sweeping with H_2 at 623°K for 34 hours	0.63 ± .03		498 ± 20	c
	1.40 ± .03	2.60 ± .03		f
	0.58 ± .03	0.92 ± .03		g
4) sweeping with H_2 at 943°K for 12 hours	0.26 ± .03		328 ± 20	c
5) iron	0.26		340	c,h
6) calcined in air at 773°K and outgassed at 573°K	0.53 ± .03	0.3 ± .05	507 ± 20	c
	0.62 ± .05	1.03 ± .02		e

Continued/.....

Table 7 Continued

[a] in mm/sec relative to sodium nitroprusside

[b] in kOe

[c] hyperfine component

[d] lines 3 and 5

[e] inner doublet

[f] lines 4 and 7

[g] lines 4 and 5

[h] reference #6

as can be seen in Figure 9a). Hence the hydrogen must be acting in some way on the ferric ion to produce the intermediate stage of Figure 9b). Subsequent outgassing then produces bulk α-Fe_2O_3 at the expense of the original ferric species in the sample.

Figure 10 shows the results of a) further treatment of the pellet with hydrogen at higher temperatures b) hydrogen treatment at 943^{o}K and finally c) calcining the pellet in air at 773^{o}K and outgassing it at 573^{o}K.

As the temperature is increased while passing hydrogen over the pellet, the central doublet slowly disappears and the intensity of the hyperfine pattern increases.

Figure 10a) shows a room temperature hyperfine pattern with an internal field similar to that expected for a ferric oxide. However the line widths are fairly broad and possibly indicative of the superposition of another six-line pattern. The asymmetry represented in the central doublet is probably indicative of the superposition of another absorption line on line 4. The isomer shift obtained by pairing lines 4 and 7 is fairly representative of Fe^{2+} compounds. Lines 3 and 6 belong to the hyperfine pattern and lines 4 and 5 to the central doublet. Table 7 lists the parameters corresponding to these combinations. The contribution of the central doublet to the overall spectrum is considerably less than in Figure 9c).

Finally sweeping with hydrogen at 943^{o}K produces the iron (Fe^{o}) spectra of Figure 10b). Bulk Fe^{o} parameters are also listed in Table 7 for comparison. Since the line-fit to the points is not very good in the region of the centroid of the

FIGURE 10

Room Temperature Mössbauer Spectra of the pellet in a vacuum:

a) pellet swept by hydrogen for 34 hours at 623°K

b) pellet swept by hydrogen for 12 hours at 943°K

c) after final hydrogen treatment pellet calcined in air at 573°K and then outgassed at 573°K

FIG 10

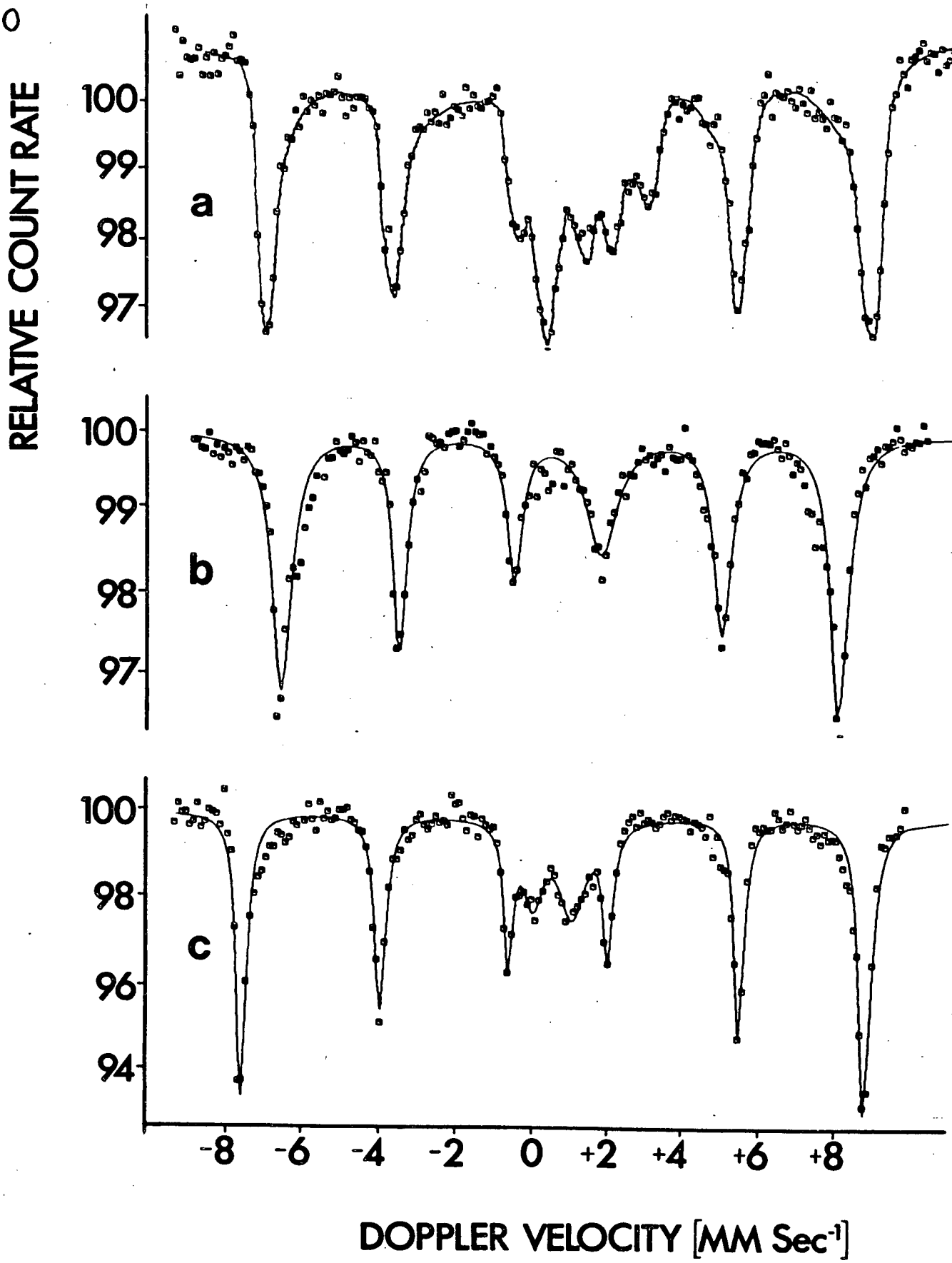
RELATIVE COUNT RATE
100
99
98
97
a
100
99
98
97
b
100
98
96
94
c
-8
-6
-4
-2
0
+2
+4
+6
+8
DOPPLER VELOCITY [MM Sec-1]

spectrum, some of the central doublet is still suspected to be present.

In order to get from the Fe^{o} spectrum of Figure 10b) to a spectrum characteristic of bulk α-Fe_2O_3 it was found necessary to calcine the pellet in air. Outgassing the Fe^{o} sample at $773^{o}K$ in a vacuum did not alter the spectrum of 10b) at all. Presumably the mechanism for the conversion requires surface water. This most probably would not be available because the sample had been heated to a higher temperature and most of the chemisorbed water driven off.

The spectrum of 10c) was obtained after calcining the sample at $773^{o}K$ in air and outgassing it at $573^{o}K$. The Mössbauer parameters for the central doublet and the hyperfine component are listed in Table 7. The parameters of the doublet are quite similar to those attributed to the doublets of the other spectra. From the hyperfine parameters, bulk α-Fe_2O_3 appears to be the predominant ferric species. The outer lines do not appear to fit the points properly and the possibility of the superposition of a second hyperfine pattern still exists.

Passing hydrogen over the sample at elevated temperatures causes the reduction of the ferric species to Fe^{o}. The mechanism for the conversion of Fe^{o} to bulk α-Fe_2O_3 seems reasonably clear. Perhaps the mechanism involved in the conversion of the "iron" species in Figure 9b) to the hyperfine spectrum of 9c) also depends on the availability of surface water.

It appears that at intermediate temperatures Fe^{2+} is produced though this cannot be said with any degree of assurance about Figure 9b). The role played by Fe^{2+} is not altogether clear.

Since the system initially exhibited a variety of relaxation times consistent with the interpretation of a magnetically dilute system, the ferric centres affected first would be those with the longest bond distances and the weakest interactions. The ferric species left contributing to the central doublet would probably have shorter relaxation times and therefore not necessarily contribute to the hyperfine pattern at $\sim 105^{o}K$ (which was the observed effect). The high temperature required to lessen the intensity of the central doublet would be consistent with the increasing energy of interaction between ferric centres. The Fe^{2+} species formed would probably readily oxidize to produce the observed magnetic hyperfine pattern at room temperature.

A great deal more work needs to be done in this area in order to determine exactly the processes that are involved in the conversion of the initial ferric species to bulk α-Fe_2O_3.

In order to insure that the temperature treatment involved in the conversion of the ferric ion to bulk α-Fe_2O_3 did not disrupt the zeolite lattice an X-ray powder photograph was taken (listed in column 4 of Table 3). Comparison with the other X-ray data shows that some structural rearrangements may have occurred but that the differences are not so great as to imply the total collapse of the zeolite framework. Column 5 in Table 3 lists the d-spacings for bulk α-Fe_2O_3. The appearance of the 5.90 line may or may not indicate the presence of α-Fe_2O_3.

A single magnetic measurement was made by the Gouy method on the reduced and outgassed sample of Figure 10c). The typical range for the value of the gram susceptibility was $\chi_g \sim (6 \rightarrow 10) \times 10^{-3}$.

This number is at least an order of magnitude greater than the original χ_g ($\sim$1 X 10^{-4}) and since hysteresis effects were also observed it was concluded that the sample showed magnetically ordered behaviour.

There was no change in the Mössbauer parameters of Figure 10c) on nitrogen adsorption.

The nitrogen isotherm of Figure 11b) was obtained on a powder sample of iron-L-zeolite that had been outgassed at 573^{o}K. The difference between this isotherm and that of Figure 11a) (the nitrogen isotherm of the 573^{o}K outgassed solvated-L-zeolite) is quite remarkable. From Table 8 it can be seen that the surface area drops from 375 m^2/gm to 98 m^2/gm. This is an extremely good indication that the iron species occluded within zeolite-L is blocking the pores.

After adsorption isotherms of CO_2 and C_2H_6 were measured; this sample was subjected to the passage of hydrogen over it at various temperatures, calcining in air and finally outgassing in a vacuum at 573^{o}K. The nitrogen isotherm of Figure 11c) was obtained. The surface area available for nitrogen adsorption has increased twofold over the initial area of iron-L-zeolite. Clearly then this is a good indication that the bulk of the α-Fe_2O_3 that is formed resides on the external surface of the zeolite. The question still remains as to how it gets there! One possible explanation is that at 943^{o}K the Fe^{o} formed may be sufficiently mobile that it diffuses out of the pores and forms aggregates on the external surface[17].

This powder sample was examined by Mössbauer spectroscopy and a spectrum whose parameters were similar to those of Figure

FIGURE 11

Nitrogen Adsorption isotherms at $77^{o}K$

8% iron content

a) on outgassed solvated-L-zeolite

b) on outgassed iron-L-zeolite

c) on outgassed iron-L-zeolite
after producing bulk α-Fe_2O_3

FIGURE 11

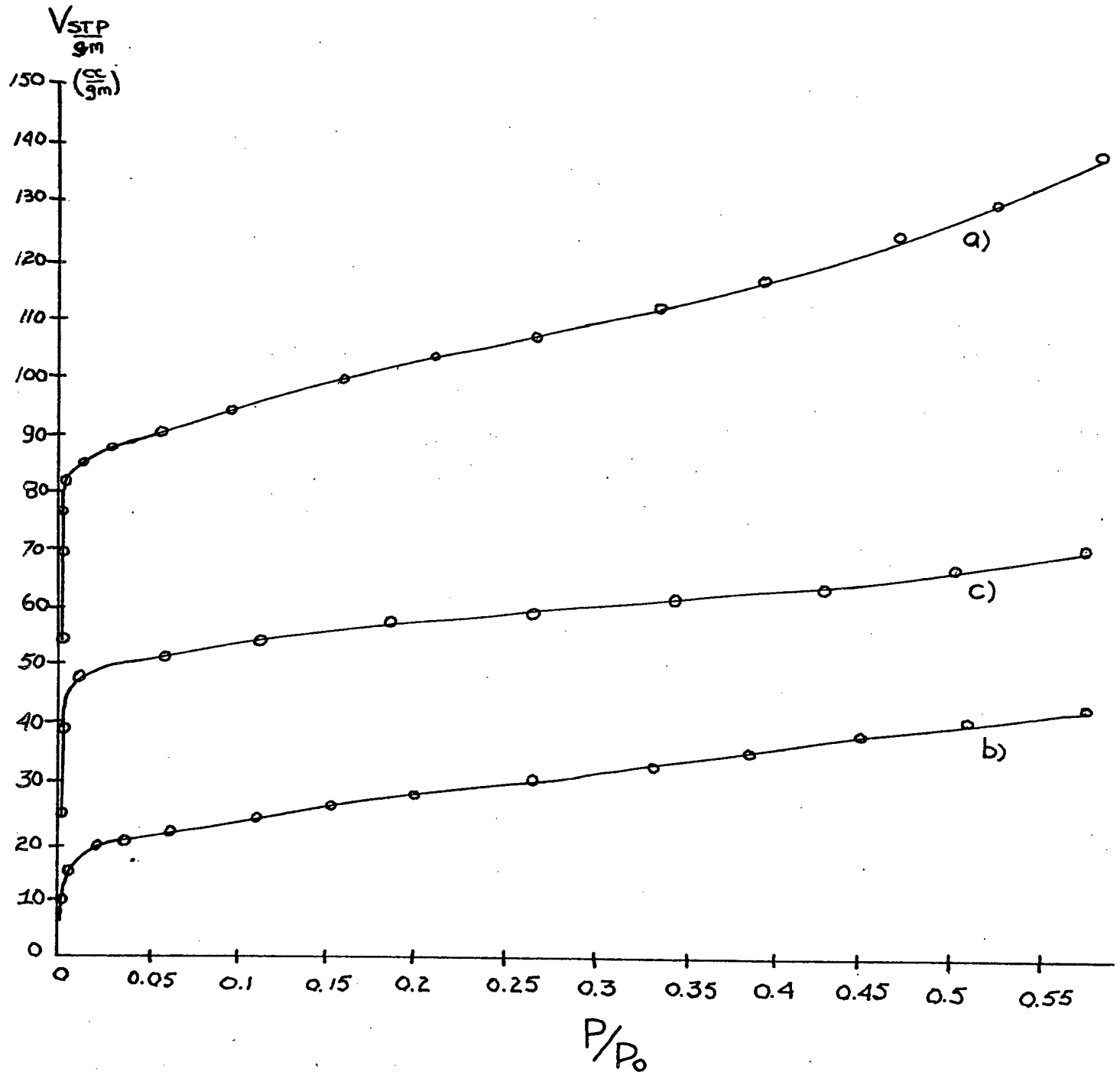
$V_{\frac{STP}{gm}}$
$(\frac{cc}{gm})$
150
140
130
120
110
100
90
80
70
60
50
40
30
20
10
0
0
0.05
0.1
0.15
0.2
0.25
0.3
0.35
0.4
0.45
0.5
0.55
P/Po
a)
c)
b)

10c) was obtained.

Figure 12 represents nitrogen adsorption isotherms on a different powder sample of iron-L-zeolite. (In this sample chemical analysis indicated that there was approximately a 9.5 percent iron content). The treatment of the sample was: a) room temperature evacuation b) outgassed at 573°K c) swept with hydrogen at 573°K and room temperature evacuated and d) outgassed at 573°K. Table 8 lists the surface areas obtained from BET plots. The surface area differences between b) and c) are within experimental error and hence virtually no change has occurred with treatment. Isotherm d) however does show a small increase in surface area.

For comparison purposes a Mössbauer spectrum was recorded for a sample of d). The spectrum obtained was identical to that of Figure 9c).

The trend toward increased surface area as bulk α-Fe_2O_3 was produced is a good indication that the pores are becoming less congested. However the question still arises as to the nature of the mobile species that permits diffusion out of the pores.

Figure 13 represents the adsorption isotherms of CO_2 and C_2H_6 on both solvated-zeolite L and on iron-L-zeolite. Comparison of the surface areas obtained with the same adsorbate between the two zeolites can be made from Table 8. In both cases the uptake of ethane is much smaller than that of either CO_2 or N_2. This demonstrates the sieving ability of the zeolites in that smaller molecules like CO_2 and N_2 have access to parts of the zeolite which are precluded to bigger molecules.

FIGURE 12

Nitrogen Adsorption isotherms on iron-L-zeolite at 77°K

9.5% iron content

a) sample evacuated

b) sample outgassed at 573°K

c) sample swept with hydrogen at 573°K then evacuated

d) sample outgassed at 573°K

FIGURE 12

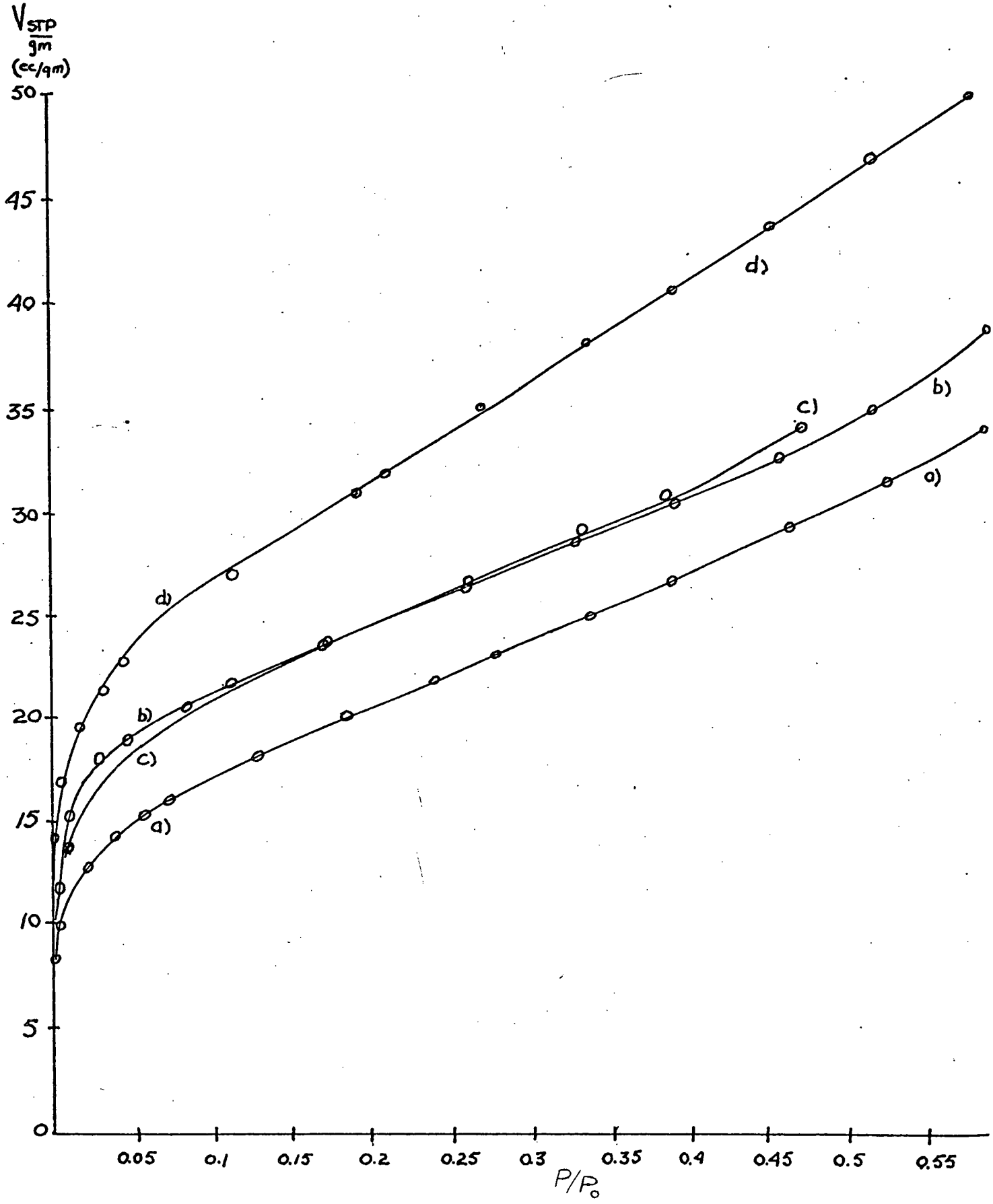
V_{STP} / gm (cc/gm)
50
45
40
35
30
25
20
15
10
5
0
0.05
0.1
0.15
0.2
0.25
0.3
0.35
0.4
0.45
0.5
0.55
P/P₀
a)
b)
c)
d)

FIGURE 13

Adsorption isotherms
at 195°K:

a) CO_2 on outgassed solvated-L-zeolite

b) C_2H_6 on outgassed solvated-L-zeolite

c) CO_2 on outgassed iron-L-zeolite

c) C_2H_6 on outgassed iron-L-zeolite

FIGURE 13

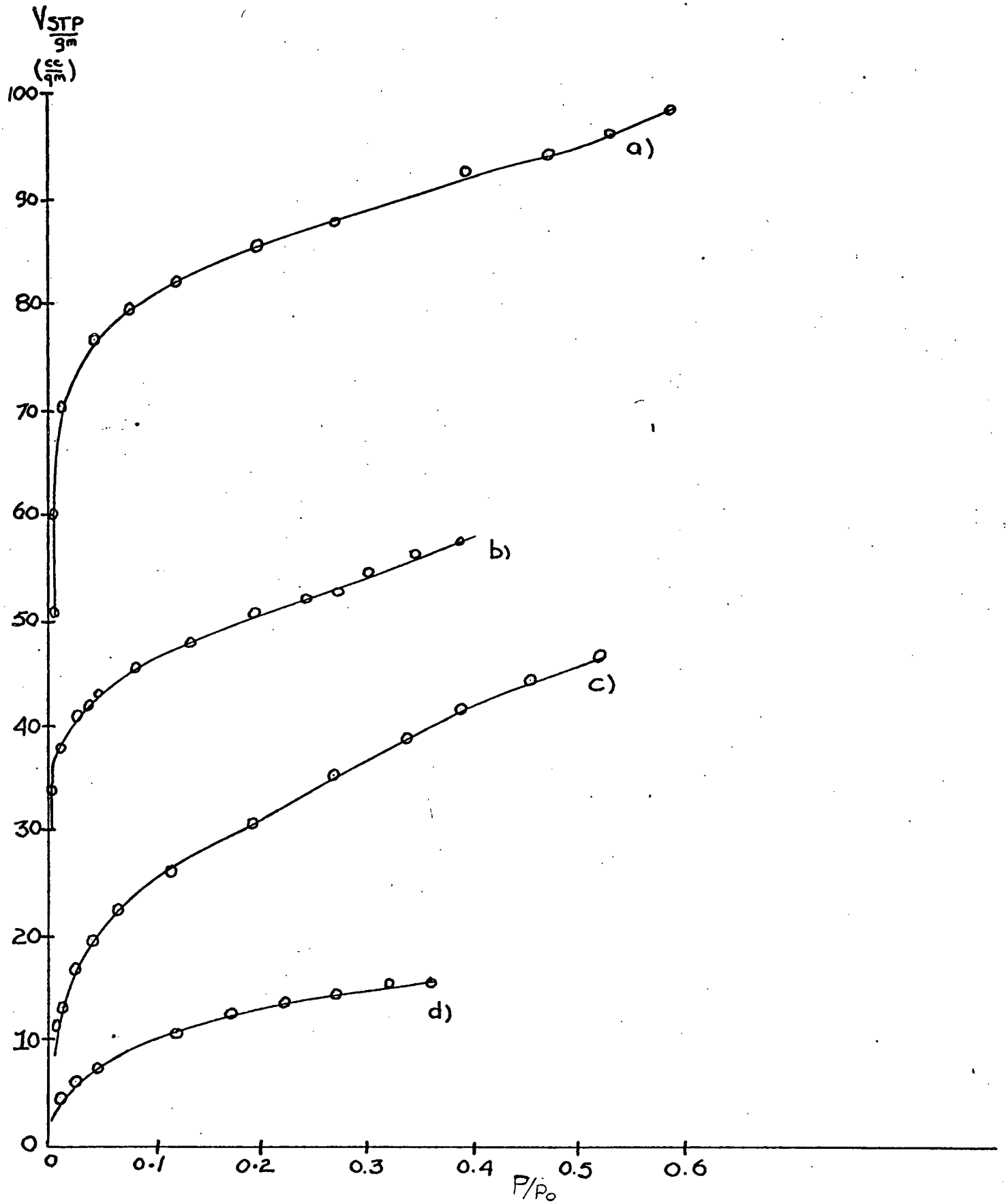
V_{STP} / gm
(cc/gm)
100
90
80
70
60
50
40
30
20
10
0
0
0.1
0.2
0.3
0.4
0.5
0.6
P/Po
a)
b)
c)
d)

The isotherms of C_2H_6 and N_2 demonstrated purely physical adsorption as can be seen by the magnitudes of the BET energies listed in Table 8. This substantiates the Mössbauer evidence. Carbon dioxide was physically adsorbed on solvated L-zeolite but on iron-L-zeolite the isotherms behaved quite unusually. As the isotherm temperature was increased the adsorption appeared to be increasing. However the gas desorbed quite readily. Since the Mössbauer Spectra showed no evidence of CO_2 altering the coordination sphere about the ferric ion it appeared unlikely that chemisorption to iron occurred. Further investigation of this peculiarity is required.

Since the energies obtained by BET plots are not really meaningful, isosteric heats for ethane on solvated L-zeolite and iron-L-zeolite are shown in Figure 14. The initial drop in the heat with coverage is quite usual because in the low coverage region sites with steadily decreasing energy are filled. The appearance of an increase and maximum in the energy on both zeolites at around monolayer coverage are probably representative of lateral interactions between adsorbate molecules occurring within the pores. This same trend was observed for carbon dioxide and ethylene on solvated zeolite-L and has been observed before by Barrer and co-workers[33].

In conclusion, the present sample contains a single ferric species as an oxyhydroxide of iron. The species behaves like a simple relaxing paramagnet down to 80°K. Adsorption studies on the untreated sample show that the iron oxyhydroxide blocks the pores of the zeolite. Temperature treatment of the sample either in air or in hydrogen frees the pores and produces

Table 8*

Sample and Treatment	Gas	Temp (^{o}K)	[c]Area $\frac{m^2}{gm}$	Energy $\frac{kcal}{mol}$
1) outgassed solvated L-zeolite	N_2	77	375	2.3
	CO_2	195	382	8.1
	C_2H_6	195	248	5.5
2)[a] iron-L-zeolite	N_2	77	98	2.1
	CO_2	195	116	7.0
	C_2H_6	195	63	5.2
3)[a] iron-L-zeolite after producing bulk α-Fe_2O_3	N_2	77	220	2.3
4)[b] iron-L-zeolite				
a) evacuated	N_2	77	75	2.0
b) outgassed	N_2	77	86	2.2
c) H_2 passed over at 573^{o}K then evacuated	N_2	77	88	2.1
d) outgassed	N_2	77	110	2.1

* outgassing temperatures were 573^{o}K

[a] sample contains 8% iron

[b] sample contains 9.5% iron

[c] experimental error limits are ± 5%

FIGURE 14

Isosteric heats of adsorption versus surface coverage for ethane on:

a) solvated-L-zeolite

b) iron-L-zeolite

FIGURE 14

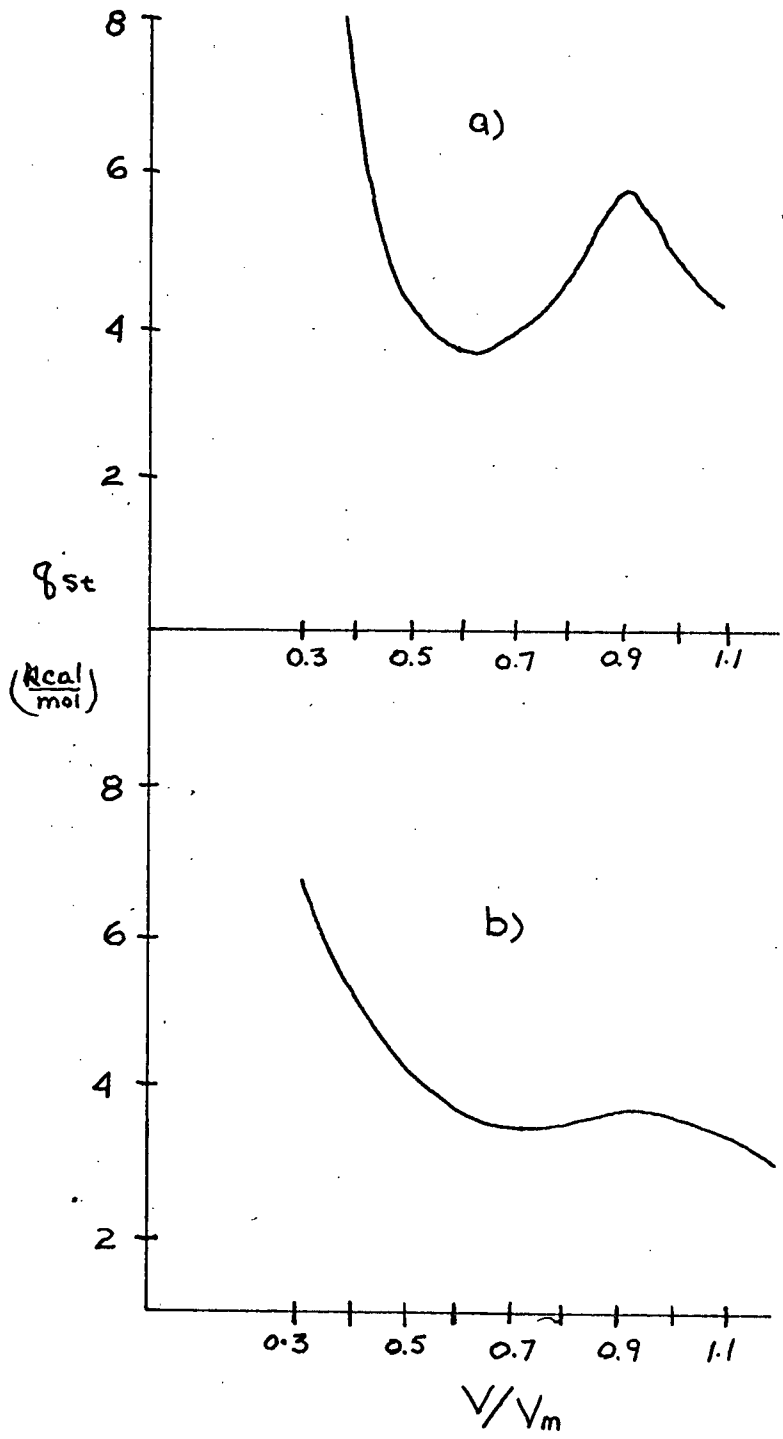

bulk α-Fe_2O_3 which by some mechanism aggregates on the external surface of the zeolite.

The Mössbauer behaviour pattern observed on this sample is in many ways much different from that reported in an earlier work by Wedd et al[17]. The primary difference appears to lie in the observation of relaxation effects in this sample, which they did not observe in theirs. Also, they reported the appearance of an Fe^{2+} species on outgassing their sample which was not observed here. Differences in the temperature at which Fe^{o} spectra were obtained were also apparent. These discrepancies may arise from the method of preparation of the sample which would prove an interesting area for further investigation.

BIBLIOGRAPHY

[1] D.W. Breck, J. Chem. Ed., 41, 678 (1964).

[2] L.V.C. Rees, Annual Reports on the Progress of Chemistry, A, 67, 191 (1970).

[3] G.K. Wertheim, "Mössbauer Effect, Principles and Applications", Academic Press, London, 1964.

[4] L.R. Walker, G.K. Wertheim, and V. Jaccarino, Phys. Rev. Letters, 6, 98 (1961).

[5] R. Ingalls, Phys. Rev., 133, 3A, 787 (1964).

[6] N.N. Greenwood, and T.C. Gibb, "Mössbauer Spectroscopy", Chapman and Hall Ltd., London, 1971.

[7] M. Blume, Phys. Rev. Letters, 14, 96 (1965).

[8] M. Blume, Phys. Rev. Letters, 18, 305 (1967).

[9] S. Brunauer "Physical Adsorption", Princeton University Press, Princeton, (1945).

[10] G.D. Halsey, Advances in Catalysis, 4, 259 (1952).

[11] T.L. Hill, J. Chem. Phys., 17, No. 6, 520 (1949).

[12] T.L. Hill, J. Chem. Phys., 18, No. 3, 246 (1950).

[13] D.M. Young, and A.D. Crowell, "Physical Adsorption of Gases", Butterworth and Co., London, 1962.

[14] W.N. Delgass, and M. Boudart, Catalysis Reviews, 2, 129 (1968).

[15] M.C. Hobson Jr., Advances in Colloid and Interface Science, 3, 1 (1971).

[16] J. Morice, and L.V.C. Rees, Trans. Faraday Soc., 64, 1388 (1968).

[17] R.W.J. Wedd, B.V. Liengme, J.C. Scott, and J.R. Sams, Solid State Commun., 7, 1091 (1969).

[18] V.I. Goldanskii, I.P. Suzdalev, A.S. Plachinda, and L.G. Shtyrkov, Proc. Acad. Sci. U.S.S.R., Phys. Chem. Sect. English Transl., 169, 511 (1966).

[19] G. Constabaris, J.H. Singleton, and G.D. Halsey Jr., J. Phys. Chem., 63, 1350 (1959).

[20] R.W.J. Wedd, M.Sc. Thesis, University of British Columbia, 1967.

[21] U.S. Patent No. 3, 130, 006, April 21 (1964).

[22] R.M. Barrer, and H. Villiger, Zeitschrift für Kristallographie, Bd. 128, S., 352 (1969).

[23] G. Constabaris, R.H. Lindquist, and W. Kündig, Appl. Phys. Letters, 7, No. 3, 59 (1965).

[24] W. Kündig, H. Bömmel, G. Constabaris, and R.H. Lindquist, Phys. Rev., 142, No. 2, 327 (1966).

[25] P.W. Selwood, "Magnetochemistry," 2nd edn., Interscience, New York, 1956.

[26] D.W. Collins, J.T. Dehn, and L.N. Mulay in "Mössbauer Effect Methodology," 3, (ed. I.J. Gruverman), Plenum Press, New York, 1967.

[27] M.J. Rossiter, A.E.M. Hodgson, J. Inorg. Nucl. Chem., 27, 63 (1965).

[28] F. van Der Woude, A.J. Dekker, Phys. Stat. Sol. 13, 181 (1966).

[29] I. Dezsi, and M. Foder, Phys. Stat. Sol. 15, 247 (1966).

[30] I. Dezsi, L. Keszthelyi, D. Kulgawczuk, B. Moinar, and N.A. Eissa, Phys. Stat. Sol. 22, 617 (1967).

[31] N. Malathi, and S. Puri, J. Phys. Soc. Japan, 31, No. 5, 1418 (1971).

[32] V.I. Goldanskii, I.P. Suzdalev, A.S. Plachinda, and V.P. Korneev, Dokl. Akad. Nauk SSSR, 185, 203 (1969).

[33] R.M. Barrer, and J.W. Sutherland, Proc. Roy. Soc., Sec. A, 237 (1956).

[34] W.W. Collins, and L.N. Mulay, IEEE Transactions on Magnetics, 4, 470 (1968).

APPENDIX

Calculation of Volume Adsorbed

The following symbols are used:

P_I initial pressure of injected gas

P_E equilibrium pressure over sample

V_p volume of pipets

V_{op} volume of overhead pipets

V_{oc} volume of overhead cell

V_c volume of cell

V_m manometer volume correction term for a given pressure (V_{mI} or V_{mE})

T_p temperature of pipets

T_R room temperature

T_c cell temperature

n_I total number of moles of gas in the system

n_E number of moles of gas remaining in the gas phase after equilibration over the sample

n_A number of moles of adsorbed gas

R gas constant

With the cell and overhead cell segments closed off from the system, the number of moles of gas initially injected is given by

$$\frac{P_I}{R}\left(\frac{V_p}{T_p} + \frac{V_{op}}{T_R} + \frac{V_{mI}}{T_R}\right) = n_I \qquad (1)$$

The cell and overhead cell segments are opened to the system, and at equilibrium

$$\frac{P_E}{R}\left(\frac{V_p}{T_p} + \frac{V_{op}}{T_R} + \frac{V_{mE}}{T_R}\right) + \frac{P_E}{R}\left(\frac{V_{oc}}{T_R} + \frac{V_c}{T_c}\right) = n_E \qquad (2)$$

The number of moles adsorbed is given by

$n_I - n_E = n_A$ at pressure P_E.

The cell and overhead cell segments are again closed and the gas pressure increased by altering the combination of the pipet volumes. After expanding the gas into the cell a new equilibrium pressure P_E^1 is obtained. The number of moles remaining in the gas phase after equilibration over the solid sample is obtained from

$$\frac{P_E^1}{R}\left(\frac{V_p^1}{T_p} + \frac{V_{op}}{T_R} + \frac{V^1_{mE}}{T_R}\right) + \frac{P_E^1}{R}\left(\frac{V_{oc}}{T_R} + \frac{V_c}{T_c}\right) = n_E^1 \qquad (3)$$

and the number of moles adsorbed at pressure p_E^1 is

$n_A^1 = n_I - n_E^1$

When gas is again injected into the system from the external storage bulbs (with the cell segments closed) the increase in the initial number of moles is obtained from the difference between the last equilibrium pressure and the new pressure

$$\Delta P \left(\frac{V_p}{T_p} + \frac{V_{op}}{T_R} + \frac{\Delta V_m}{T_R} \right) = \Delta n$$

and the total moles of gas in the system is given by

$$n_t = n_I + \Delta n.$$

The volume adsorbed at temperature T_c and equilibrium pressure P_E is given by

$$Vads = n_A \frac{RT_c}{P_E} \qquad (6)$$

At standard temperature (T_S) and pressure (P_S) this becomes

$$V_{STp} = \frac{T_S P_E}{P_S T_C} Vads$$

$$= \frac{RT_S}{P_S} n_A$$

A computer programme was written to obtain the number of moles of gas adsorbed at each equilibrium pressure and to convert these into V_{STP} values.